JOURNAL OF GEOPHYSICAL RESEARCH, VOL. 98, NO. A9, PAGES 15,643–15,665, SEPTEMBER 1, 1993

The Role of Ducted Whistlers in the Precipitation Loss and Equilibrium Flux of Radiation Belt Electrons

W. C. BURGESS[1] AND U. S. INAN

Space, Telecommunications and Radioscience Laboratory, Stanford University, Stanford, California

New experimental evidence suggests that every ducted whistler component may precipitate bursts of radiation belt electrons into geomagnetically conjugate ionospheric regions. Strong spatial and temporal associations are seen between transient ionospheric disturbances observed in conjugate regions and ducted whistlers monitored at Palmer Station, Antarctica. The ionospheric disturbances were detected by their characteristic perturbing effects ("Trimpi events") on subionospheric VLF, LF, and MF signals recorded at Palmer Station and at northern hemisphere sites. Of 74 such events examined on four different days, all were time-associated with ducted whistlers. In no case was the arrival azimuth or dispersion of the associated whistlers inconsistent with the locations of the conjugate ionospheric disturbances, which were inferred from the configuration of perturbed signal paths. Other whistlers occurring independently of detected disturbances were found to be either weak or to have arrived from regions where a disturbance would not have been detected for lack of monitored signal paths. Signal perturbation onset behavior was consistent with multiple regions of precipitation induced by components of multipath whistlers and with theoretical predictions for ducted whistler-induced precipitation. The results not only support the hypothesis that ducted whistlers are responsible for burst precipitation of energetic electrons but imply that such bursts may be induced by every ducted whistler component. Since radio energy from a lightning discharge can excite whistler ducts located 2500 km or more away from the flash, every ducted whistler observed at Palmer Station may indicate the presence of precipitation bursts associated one-to-one with excited whistler ducts distributed over a 5000-km-wide portion of the Earth's surface, and over its geomagnetic conjugate as well. The estimated effect of this precipitation on 70- to 200-keV radiation belt electron populations for $2 < L < 3$ is comparable to that predicted as a result of plasmaspheric hiss, indicating that ducted whistlers may contribute as significantly as hiss to radiation belt equilibrium at those electron energies.

1. INTRODUCTION

Since 1963, certain transient perturbations of subionospheric VLF, LF, and MF signals, sometimes called "Trimpi events," have been known to occur in association with ground-based observations of whistlers generated by atmospheric lightning. These perturbations of signal amplitude and phase, characterized by a sudden onset and a roughly exponential recovery lasting about 1-min, were attributed by *Helliwell et al.* [1973] to secondary ionization in the lower ionosphere caused by whistler-associated precipitation of energetic radiation belt electrons, a phenomenon now often referred to as lightning-induced electron precipitation (LEP). This hypothesis has been supported by many later studies [e.g., *Lohrey and Kaiser*, 1979; *Inan and Carpenter*, 1987] and by in situ observations [*Rycroft*, 1973; *Voss et al.*, 1984; *Goldberg et al.*, 1987].

The role played by whistler ducts in electron precipitation is less well understood. Whistler ducts are thought to be enhancements of ionization aligned with the geomagnetic field, extending between the hemispheres and capable of guiding VLF waves with wave normal vectors nearly parallel to the field (see *Strangeways* [1991] for a recent treatment of whistler duct structure). The existence of ducts is consistent with the propagation of ground-observed whistlers along magnetic field lines and through the magnetosphere-ionosphere boundary without suffering total internal reflection [*Helliwell*, 1965]; however, in situ evidence of ducts is extremely limited [*Angerami*, 1970]. Although *Inan et al.* [1985*b*] assumed ducted wave propagation in a model of electron scattering by whistler-mode VLF transmitter signals, they found that predictions for scattering by both ducted and nonducted signals generally agreed with corresponding S81-1 satellite measurements of precipitating ~18-keV electrons. A study of VLF transmitter-induced precipitation by *Vampola* [1987] established that the distribution of 235-keV electron pitch angles observed on the S3-3 satellite was consistent with scattering either by field-aligned ducted waves above the ionosphere or by nonducted interactions very low on the field line. *Inan et al.* [1989] noted that the spatial extent of lightning-associated >45-keV precipitation bursts detected by the S81-1 satellite, as reported by *Voss et al.* [1984], is difficult to reconcile with scattering confined to a whistler duct.

Despite these concerns, ducted whistler waves are often assumed to be the primary scattering agent in lightning-induced precipitation of $\gtrsim$50-keV electrons. This is due in part to the efficiency with which such electrons are thought to be scattered by ducted whistlers [*Inan et al.*, 1989], but also in part to the reliable observation of ducted whistlers in association with the characteristic signal perturbations just mentioned; for example, after over 300 comparisons of signal perturbations and broadband whistler data recorded on over 20 different days at Palmer Station, Antarctica, the authors have yet to find a characteristic perturbation not accompanied by a ducted whistler. Additional evidence consistent with a cause-effect relationship between ducted whistlers and electron precipitation was presented by *Carpenter and LaBelle* [1982] and *Inan and Carpenter* [1986] in case studies of time and magnitude correlations between whistlers and signal perturbations.

A new means to investigate the association between ducted whistlers and electron precipitation on a global scale stems from the discovery that whistler-associated ionospheric disturbances can occur almost simultaneously (within 1 s) in geomagnetically con-

[1]Now at the Woods Hole Oceanographic Institution, Woods Hole, Massachusetts.

Paper number 93JA01202.
0148-0227/93/93JA-01202$05.00

jugate regions [*Burgess and Inan*, 1990]. In this paper we analyze such disturbances using high-time resolution conjugate recordings of subionospheric signal perturbations and compare these with the multipath structure, arrival azimuths, and predicted electron scattering effects of associated whistlers. This analysis provides us with more comprehensive evidence of the scattering and bounce behavior of whistler-associated precipitation bursts than was heretofore available. The results of the study not only support a strong link between individual whistler ducts and conjugate ionospheric disturbances, but imply that every ducted whistler component precipitates electron bursts and that such precipitation significantly influences the equilibrium of the radiation belts.

2. DESCRIPTION OF THE PHENOMENON

Precipitation bursts responsible for lower ionospheric disturbances are thought to be induced when a magnetospheric wave propagating in the whistler mode undergoes cyclotron resonance with radiation belt electrons traveling in the opposite direction, scattering them in pitch angle [*Dungey*, 1963; *Cornwall*, 1964]. ELF and VLF whistler mode signals can resonate with quasi-relativistic electrons of energies ranging from 50 to 500 keV or more. If scattered into the bounce loss cone, these electrons are capable of penetrating the atmosphere to altitudes as low as 60 km [*Rees*, 1963]. When scattered by a southbound whistler, a precipitation burst would first encounter the northern hemisphere ("direct precipitation"). Upon reaching the atmosphere, up to 90% of the burst electrons could backscatter due to their grazing angles of incidence [*Berger et al.*, 1974] and would return along the field line to encounter the southern hemisphere. If there is an asymmetry between northern and southern mirror heights, such as that caused by the South Atlantic magnetic anomaly, a portion of the direct burst would mirror and also return to precipitate in the south without having first reached the atmosphere in the north. Precipitation bursts made up of backscattered and mirrored electrons are termed "reflected precipitation." Repeated backscattering and mirroring in both hemispheres appear to extend the lifetimes of precipitation bursts to several bounce periods [*Inan et al.*, 1985*b*; *Voss et al.*, 1984].

Figure 1 shows the sequence of events in which LEP results in lower ionospheric disturbances. Although LEP is frequently illustrated this way for convenience, there are at least two important ways in which the phenomenon may vary from that shown in the diagram. First, the lightning discharge need not be near the duct entrance and indeed could be many hundreds or even thousands of kilometers away [*Carpenter and Orville*, 1989; *Yip et al.*, 1991]; second, at the longitudes of the South Atlantic magnetic anomaly (approximately 95°W to 20°E) which are involved here, the first significant impact of precipitation on the atmosphere may occur in the south [*Inan et al.*, 1988*c*; *Burgess and Inan*, 1990].

Transient disturbances of the lower ionosphere induced by precipitation can in turn perturb VLF, LF, and MF signals propagating in the Earth-ionosphere waveguide (Figure 2). Such disturbances near the great circle transmitter-to-receiver path of a signal can change the relative amplitudes and phases of the signal's constituent modes, resulting in a sudden amplitude increase or decrease and/or a sudden phase advance or delay in the signal observed at the receiver [*Poulsen et al.*, 1993]. This initial change of amplitude or phase typically takes place over a period, called the "onset duration," of 0.5 to 1.5 s. *Inan et al.* [1985*a*] have interpreted onset duration as an indication of the length of time during which secondary ionization is produced in the ionosphere by the burst of precipitating electrons.

Signal perturbation onsets are followed by a roughly exponential recovery to ambient signal conditions. Recovery times vary but a return to ambient within 100 s is common. Recovery time may reflect ionospheric attachment and recombination chemistry at the altitudes to which precipitation bursts penetrate: *Inan et al.* [1988*a*] found agreement between observed recovery behavior and predictions from a first-order model of ionizing burst penetration altitudes and corresponding effective recombination rates.

The lightning discharge with which signal perturbations are associated generates a radio atmospheric, or "sferic," (Figure 1), which is often strong enough to be detected as an amplitude impulse on narrow-band as well as broadband VLF recordings [*Inan et al.*, 1988*b*]. When this "causative sferic" can be identified, the delay between it and the onset of the associated signal perturbation is called the "onset delay." *Lohrey and Kaiser* [1979] linked onset delays to magnetospheric parameters, including L shell and cold plasma electron density, which control the time required for significant whistler-electron interactions to begin. Later studies by *Carpenter et al.* [1984] and *Inan et al.* [1985*a*] have supported this interpretation. Commonly observed onset delays range from 0.3 to 1.6 s.

Recent work has suggested that signal perturbation data can be used to "image" the locations of ionospheric disturbances. Experimental evidence implies that signal perturbations are caused by disturbances within 100 km of the signal path [*Inan et al.*, 1990]. *Poulsen et al.* [1990] have designed a model of subionospheric VLF propagation and scattering, based on realistic three-dimensional waveguide mode simulation as opposed to ray superposition, which suggests that an ionospheric disturbance would not perturb subionospheric VLF signals whose paths lie more than 250 km away from the disturbance center. As indicated in Figure 3, the effect of atmospheric noise on the signal receivers often means that signal amplitude perturbations less than 0.05 dB cannot be distinguished, so in practice only disturbances within ~200 km of a signal path would detectably perturb it. These results suggest that the location of an ionospheric disturbance's center can be estimated to lie within 200 km of the perturbed signal paths. The horizontal extent of typical disturbances was estimated by *Carpenter and LaBelle* [1982] and *Inan et al.* [1990] to be of the order of 100 km or less.

3. DATA ACQUISITION AND ANALYSIS

The data presented in this paper are composed of narrow-band recordings of sferics and subionospheric signal amplitudes, monitored at a number of sites, and simultaneous broadband VLF recordings of whistlers and sferics from Palmer Station, Antarctica. Table 1 lists the transmitters monitored and Table 2 lists the receiving sites. In the following discussion, signal paths and receiving sites are referred to by abbreviation; for example, NPM–PA denotes the NPM to Palmer Station signal path. All signal paths referred to in this paper are assumed to describe a great circle arc. A global view of the signal paths is shown in Figure 4. Locations of geomagnetic conjugates and L shells were obtained using the model of *Tsyganenko* [1989]. Timing for all data was obtained from the Geostationary Operational Environmental Satellite (GOES) with an accuracy of ±2.0 ms. Broadband and narrow-band measurements at Palmer Station were made with two orthogonal 78 m^2 loop antennas aligned to local magnetic north-south and east-west. Narrow-band measurements at other sites relied on single, smaller loop antennas.

VLF and LF signals were monitored using narrow-band receivers. The 500-Hz bandwidth of these receivers passes most of

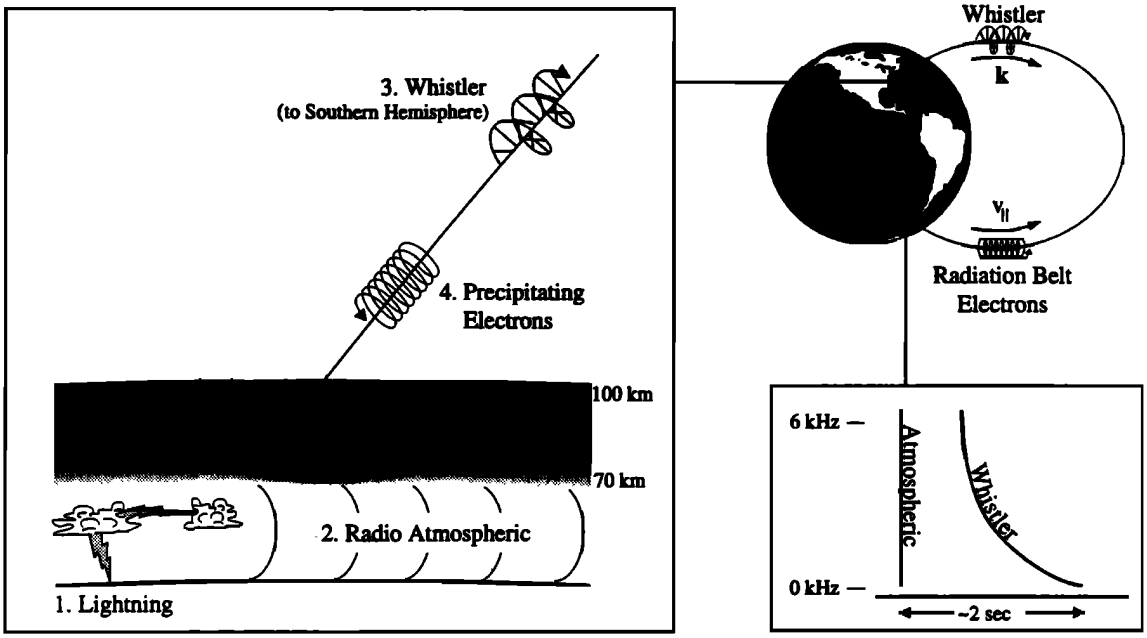

Fig. 1. Electron precipitation induced by ducted whistlers. A lightning discharge (1) launches a radio atmospheric, or "sferic" (2), which propagates in the Earth-ionosphere waveguide and is often strong enough to be detectable all over the planet. Enhancements of the plasma above the ionosphere, aligned with the geomagnetic field and known as "ducts," can trap a portion of the sferic energy and cause it to propagate along a field line to the opposite hemisphere as a whistler (3). During its journey the circularly polarized whistler can interact with gyrating energetic radiation belt electrons, scattering them in pitch angle so that some escape from their geomagnetic trap (4). Upon striking the ionosphere, the precipitating electrons cause significant secondary ionization (5). Meanwhile, the whistler emerges from its duct and can be observed, along with the subionospherically propagating "causative" sferic, with broadband VLF radio equipment in the opposite hemisphere.

the energy in minimum shift keying (MSK) and frequency shift keying (FSK) modulated signals [*Wolf*, 1990]. MF (AM radio) signals were acquired with narrower (200 Hz) filtering to isolate the AM carrier. The detected envelopes of all receiver outputs were sampled at 100 Hz, then averaged on site to obtain lower effective sampling rates of 10, 20, or 50 Hz.

Whistler Analysis

The L shell and equatorial electron density (N_{eq}) associated with whistler ducts were determined from broadband VLF whistler dispersion measurements using the recent analytical approach of *Daniell* [1986*a*,*b*], with corrections, in a Marquardt least squares parameter estimation [*Press et al.*, 1988] (corrections to *Daniell* [1986*b*] include the replacement of $f_{H_{\min}}$ by $(f_{H_{\min}})^{\frac{1}{2}}$ in the expression for $D(f)$, and the insertion of $(f_{H_{\min}})^{\frac{1}{2}}$ after c in the expressions for $f_{N_{eq}}$. A useful approximation unmentioned in the paper is $G_2 \approx -\frac{1}{2}D_0(1 - A)$, which reduces the number of parameters to match from four to three). The Marquardt technique has been applied to whistler curve fitting before [see *Tarcsai et al.*, 1989 and references therein].

Above $L = 3$, *Strangeways et al.* [1982] observed discrepancies between whistler L values determined from dispersion analysis on the one hand and from direction-finding measurements on the other. While they attributed these discrepancies to whistler leakage from the sides of ducts in the vicinity of the duct exit regions, they also noted that the effect appeared to diminish with decreasing L. Since our data were obtained near $L = 2$, we will assume for the purposes of this paper that ducted whistlers remain at the same L shell along their entire path.

Whistler arrival azimuths at Palmer Station were measured using fast Fourier transform (FFT) comparisons of whistler amplitudes and phases from the two orthogonal antennas, a technique inspired by *Cousins* [1972]. For each of several points along a whistler trace on the frequency-time plane, the angle of the major axis of the polarization ellipse observed on the antennas was determined and weighted by the intensity of the whistler at that point. The weighted samples from the whole whistler trace were then summed to form a polar plot of arrival azimuth for that whistler. The use of only two antennas leads to a 180° ambiguity in results, but analysis of whistler L shells was in general sufficient to resolve the ambiguity. The technique enjoys better noise and multipath immunity than goniometer methods [*Cousins*, 1972]; yet, even with these advantages, difficulties persist when analyzing densely packed whistler components because of spectral leakage and time resolution limitations.

Whistler azimuth measurements suffer from polarization and multiple ray errors, which become significant when the whistler exit point is within 1000 km of the receiver; however, averaging measurements over the bandwidth of the whistler generally reduces such errors to less than 10° [*Strangeways*, 1980; *Strangeways and Rycroft*, 1980]. Since the antenna orientation uncertainty was ±5°, we estimate worst-case absolute azimuth error to be less than 15°. The technique was checked using comparisons of known and measured arrival azimuth for various Omega transmitters, with agreement in all cases being within ±5°. Arrival azimuths are given as degrees clockwise from geographic north.

Whistler intensity measurements were made using data from the magnetic north-south loop antenna. All intensity values quoted reflect peaks observed in whistler traces between 3 and 6 kHz using spectral analysis with a frequency resolution (Δf) of 61 Hz and have an error of ±25%. Unless otherwise indicated, the intensity given for a multipath whistler is that of the strongest component. Broadband data are attenuated above 9 kHz by 20 dB to prevent recorder saturation by Omega signals in the 10- to 14-kHz band.

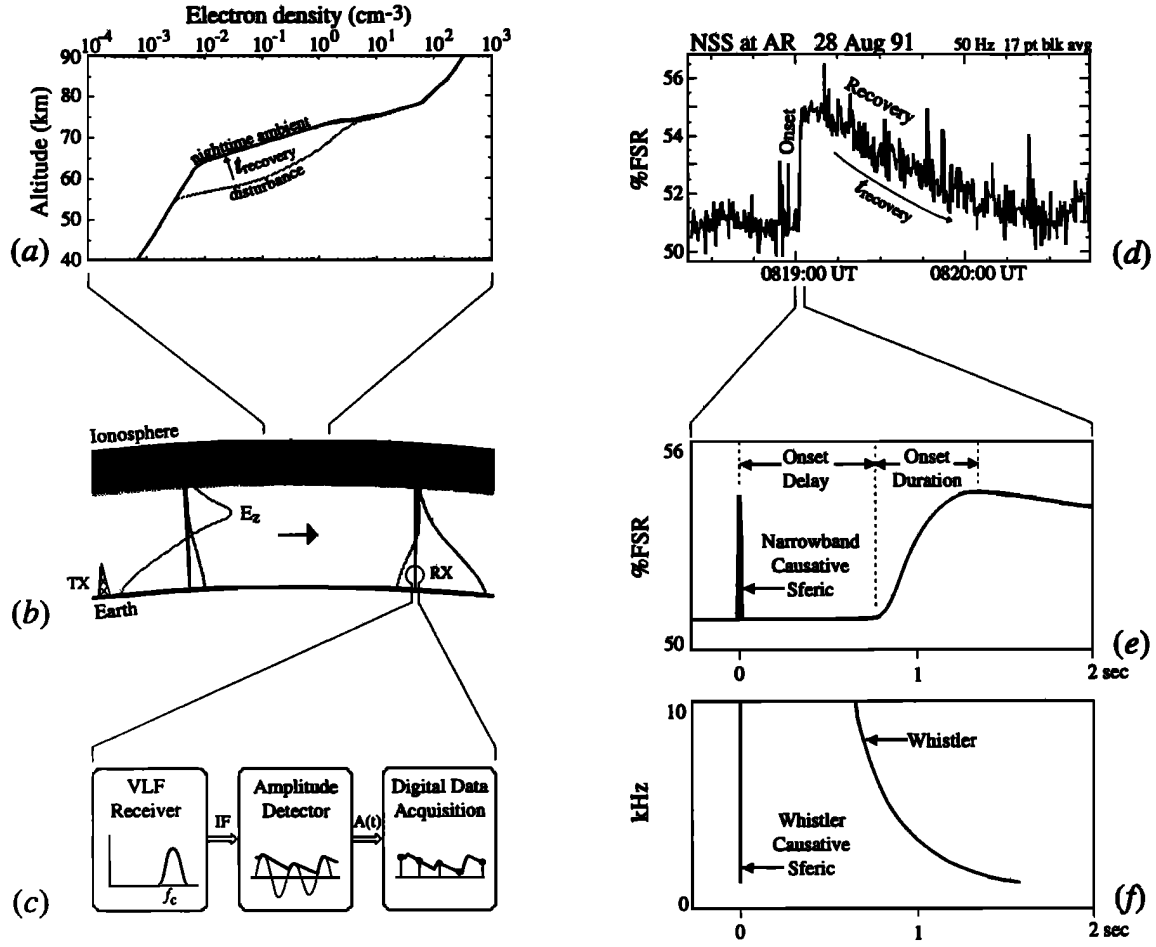

Fig. 2. Remote sensing of transient ionospheric disturbances using subionospheric VLF radio. (*a*) Electron precipitation disturbs the ambient nighttime density profile of the ionosphere. The profile recovers to the ambient over about 1 min. (*b*) The disturbance changes the relative amplitudes and phases of the Earth-ionosphere waveguide modes which constitute a subionospheric VLF signal propagating nearby. The vertical electric field (E_z) components of two possible modes are illustrated. (*c*) The subionospheric signal is acquired with a narrow-band VLF receiver, whose intermediate frequency (IF) output is amplitude detected. The resulting signal amplitude $A(t)$ is sampled and recorded. (*d*) The signal amplitude perturbation caused by the ionospheric disturbance appears as an upgoing or downgoing onset followed by a roughly exponential recovery to the ambient signal level. When calibration is unavailable, signal amplitudes are given as a percent of the recording limit, or "full-scale range" (FSR), of the acquisition system. NSS is the transmitter, AR is the receiver (see the abbreviations in Tables 1 and 2). (*e*) The causative sferic (see Figure 1) is often strong enough to be detectable in the narrow-band record when the perturbation onset is examined closely and provides a time reference for comparison with the associated whistler (*f*). The sferics in (*e*) and (*f*) are shown arriving at their respective receivers simultaneously, but the difference in propagation delay can be 40 ms or more when the narrow-band and broadband receivers are in opposite hemispheres.

Identifying Whistler-Perturbation Associations

We associate a whistler with a VLF signal perturbation in two ways. The preferred method, illustrated in Figures 2*e* and 2*f*, is based on the identification of a perturbation-associated "causative" atmospheric in the narrow-band data [*Inan et al.*, 1988*b*] which coincides, allowing for propagation delay, with a whistler causative atmospheric observed in the southern hemisphere broadband data [*Carpenter and Smith*, 1964]. When narrow-band signatures of causative atmospherics are not available, the whistler is considered to be associated with a signal perturbation if its descending frequency crosses 4 kHz within ±0.5 s of the steepest part of the perturbation onset, a threshold selected for ease of identification and for consistency with previous predictions [*Chang and Inan*, 1985] and observations [*Inan and Carpenter*, 1986]. Causative atmospherics identified in narrow-band data will henceforth be called "narrow-band causative sferics," while those identified in broadband data by their association with whistlers will be called "whistler causative sferics."

4. ASSOCIATION OF WHISTLERS AND VLF SIGNAL PERTURBATIONS

Whistlers and Northern Hemisphere Signal Perturbations

The association of signal perturbations and whistlers recorded at Palmer Station is well documented [*Inan and Carpenter*, 1986]. Palmer Station whistlers have also been associated with perturbations measured simultaneously at Palmer Station and in the northern hemisphere [*Burgess and Inan*, 1990].

Even when no signal perturbations are observed at Palmer Station, Palmer Station whistlers can be associated with northern hemisphere perturbations. Figure 5 shows a 10-min period of northern hemisphere signal perturbations occurring between 0650 and 0700 UT on April 26, 1990. During this period narrow-band data were available from AR, HU, and PA. Except for 48.5–AR, 48.5–HU, NLK–AR, NLK–HU, and NPM–HU, which were perturbed simultaneously, no other signal path observed was clearly perturbed, including NAU–HU. This configuration is consistent

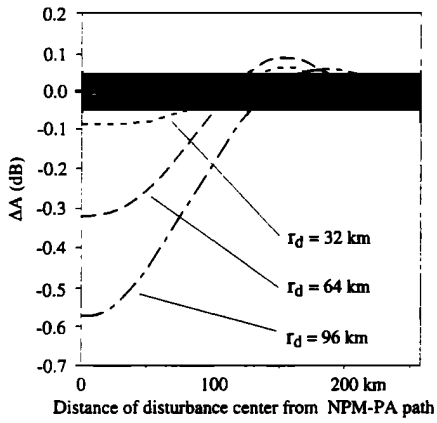

Fig. 3. Variation of the signal perturbation magnitude ΔA with the distance separating an idealized ionospheric disturbance from the NPM–PA signal path 3000 km from PA, based on a theoretical model of VLF signal propagation in the Earth-ionosphere waveguide by *Poulsen et al.* [1990]. Curves are shown for three different values of effective disturbance radius r_d. Atmospheric noise tends to obscure signal perturbations smaller than about 0.05 dB, as indicated by shading. The model suggests that disturbances more than 200 km away from the signal path are unlikely to detectably perturb it.

with an ionospheric disturbance located 100–200 km northwest of HU, as suggested in Figure 5*b*. Of the 14 0.1-dB or greater signal perturbations measured on 48.5–HU, all were associated with whistlers recorded at Palmer Station.

As narrow-band causative sferics existed in some of the northern hemisphere signal data, most clearly on NAA–HU, associated whistlers were identified by comparing the time of narrow-band and whistler causative sferics as described earlier. Narrow-band causative sferics were identifiable for 12 of the 14 perturbations of 48.5–HU. Assuming the lightning occurred over the continental United States, a reasonable assumption given the strength of the narrowband sferics at HU, the sferic propagation delay to Palmer Station would be 39 ± 5 ms. Allowing for this delay, all 12 narrow-band sferics corresponded to whistler causative sferics: in five cases the sferics matched within 20 ms (the resolution limit of the narrow-band sampled data), and even in the worst two cases the match was within 140 ms. The lack of a better match in the latter cases may represent misidentification of the causative sferics because of their tendency on this day to occur in clusters. Nevertheless, assuming that the occurrence interval between the 250 whistlers measured above ~2 μV/m in this 10-min period followed a Poisson distribution [*Inan and Carpenter*, 1986], the probability of chance association of the 12 narrow-band causative sferics within even 140 ms of whistler causative sferics would be less than 10^{-15}. As shown in Figure 6, the magnitude of the 14 northern hemisphere signal perturbations correlated with the intensity of associated whistlers, a characteristic of southern hemisphere perturbation-whistler associations reported by *Carpenter and LaBelle* [1982] and *Inan and Carpenter* [1986].

The whistlers in this case include the weakest yet documented in association with signal perturbations. The 14 associated whistlers measured between 2 and 21 μV/m, ranging below the association thresholds of 13 μV/m [*Carpenter and LaBelle*, 1982] and 50 μV/m [*Inan and Carpenter*, 1986] discussed in two previous case studies. At the same time, 42 of the total 250 whistlers observed were stronger than 50 μV/m but were not associated with detected signal perturbations in either hemisphere. The dispersion and multipath characteristics of these unassociated whistlers differed from those of the associated whistlers. Arrival azimuths could not be obtained for associated whistlers due to their weak intensities, but the unassociated whistlers appeared to arrive from azimuths of 210° to 240°, well south of the region conjugate to the 48.5–HU path. Attempts to determine precise L shell and N_{eq} of both associated and unassociated whistlers were inconclusive for lack of sufficient dispersion, due apparently to fast propagation outside the plasmapause and at low L shell ($2 \lesssim L \lesssim 2.5$). This interpretation is consistent with the strong geomagnetic activity (Kp = 5+) observed during this period (D. L. Carpenter, private communication, 1992), as well as with the relatively short onset delays of 0.2 to 0.8 s which characterized the northern hemisphere signal perturbations [*Chang and Inan*, 1985; *Burgess and Inan*, 1990].

TABLE 1. Transmitters

Call Sign	Transmitter	Modulation	Carrier, kHz	Position	Azimuth at PA[a]
	Ω Argentina	CW[b]	12.9	43°S 65°W	357.8°
NSS	US Navy Maryland	MSK	21.4	39°N 76°W	350.1°
NPM	US Navy Hawaii	MSK	23.4	21°N 158°W	275.9°
NAA	US Navy Maine	MSK	24.0	45°N 67°W	357.6°
NLK	US Navy Washington	MSK	24.8	48°N 122°W	318.5°
NAU	US Navy Puerto Rico	MSK	28.5	18°N 67°W	[c]
	US Air Force Nebraska		48.5	42°N 98°W	[c]
LU14	Río Gallegos, Argentina	AM	830	52°S 69°W	345.8°
CD96	Punta Arenas, Chile	AM	960	53°S 71°W	339.9°

[a] Given in degrees clockwise from true north.
[b] Ten-second cycle of eight pulses, four on frequency shown.
[c] Signals as observed at Palmer Station were weak, not used in azimuth study.

TABLE 2. Receivers

Site	Location	L	Position	Transmitters Monitored
AR	Arecibo, Puerto Rico	1.34	18°N 67°W	NSS, NPM, NAA, NLK, NAU, 48.5
HU	Huntsville, Alabama	2.13	35°N 87°W	NSS, NPM, NAA, NLK, NAU, 48.5
LM	Lake Mistissini, Québec	4.71	50°N 75°W	NSS, NPM, NAA, NLK, NAU, 48.5
PA	Palmer Station, Antarctica	2.42	65°S 64°W	NSS, NPM, NAA, NLK, ΩARG, LU14[a], CD96[b]

[a] LU14 was off the air for all cases except April 2, 1990.
[b] NAU and 48.5 were also monitored at PA but were too weak for useful analysis.

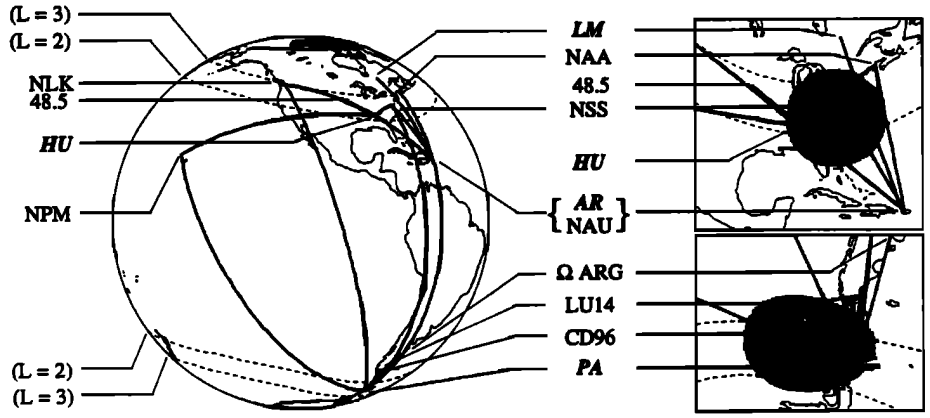

Fig. 4. The great-circle paths of signals monitored for this experiment. The transmitters are listed in Table 1, and the receivers are listed in Table 2. The right-hand panels show closeups of the path segments discussed in this paper. The shaded areas indicate a 2000-km diameter region in the northern hemisphere and its geomagnetic conjugate in the southern hemisphere, representing zones which have a relatively high "conjugate coverage" of monitored signal paths.

The association of extremely weak whistlers with signal perturbations in this case could be due to precipitation by ducted whistlers which entered the Earth-ionosphere waveguide at a relatively large distance from Palmer Station. The southern conjugate of the inferred precipitation region, where we assume precipitation-inducing ducted whistlers would exit the magnetosphere (see section 3), lies some 2300 km from Palmer Station (Figure 5*b*). Using an estimate for subionospheric VLF attenuation discussed later in section 7, propagation to Palmer Station over this distance would have attenuated the whistlers by ~36 dB.

Upon closer examination, very slight NPM–PA perturbations (<0.1 dB) can be seen in Figure 5 which coincided with many of the events on 48.5–HU. These perturbations may have resulted from nearly simultaneous ionospheric disturbances conjugate to those inferred in the north. Such disturbances would have been located some 200–250 km off the NPM–PA path, as suggested in Figure 5*b*. If this were the case, the extremely small NPM–PA perturbations compare well with the theoretical analysis by *Poulsen et al.* [1990] of diminishing perturbation magnitudes with increasing path-disturbance separation (Figure 3). By the same token, the frequent occurrence of NPM–PA perturbation magnitudes ranging from 0.1 to 1 dB and above on other days [*Wolf and Inan*, 1990] would be due to disturbances closer to the NPM–PA path.

The above results suggest that very weak observed whistler intensities are not in themselves adequate to discount the possibility of associated precipitation in either hemisphere. Whistlers at the lower limits of reception, which would include weak components of multipath whistlers, can indicate the precipitation of radiation belt electrons at locations relatively distant from the receiver.

Signal Perturbation Signatures and Multipath Whistlers

If every ducted whistler induces a precipitation burst, we would expect multipath whistlers to induce multiple precipitation bursts, causing multiple ionospheric disturbances. The disturbance of multiple regions was an interpretation offered by *Carpenter et al.* [1984] to explain the simultaneous perturbation of signals arriving at Palmer Station from widely separated azimuths. Since then, however, the possibility of multiple, simultaneous whistler-associated disturbances has not been addressed in detail.

New support for a "shotgun" model of whistler-induced precipitation, where energy from a single lightning flash scatters and precipitates electrons in multiple, distributed whistler ducts, arises from an analysis of unusual signal perturbation signatures observed on April 16, 1990. Figure 7 shows eight of the nine signal paths affected during an eleven minute period of simultaneous perturbations observed on this day at AR, LM, and PA. Data from HU were unavailable. Each of the 13 events marked *a* through *m* on NPM–PA was associated with a multipath whistler recorded at Palmer Station. The marked perturbation signatures fall into three categories: upgoing with anomalously long onset duration (~10 s), displayed by events *a* and *i*; momentarily downgoing but then upgoing (similar to the "overshoot" effect discussed by *Dingle and Carpenter* [1981]), displayed by events *b*, *c*, *e*, *g*, and *k*; and downgoing with fast (~10 s) recovery, displayed by events *d*, *f*, *h*, *j*, *l*, and *m*.

We compare the onsets of representative events *a*, *k*, and *f* with spectrograms of their associated whistlers in Figure 8. These and all multipath whistlers detected during the period included the same components, schematically identified in Figure 9. Although the relative intensity of the components differed from whistler to whistler, the dispersion characteristics remained the same. The observed variations in relative component intensity from one whistler to the next could reflect changes in the relative coupling efficiency of the causative sferic into the various whistler ducts. Such changes may in turn depend on the location and orientation of the source lightning discharge, since those characteristics would affect the sferic propagation and mode structure in the duct coupling regions.

The apparent dependence of perturbation signature on the relative component intensities of associated multipath whistlers, suggested by Figure 8, may be due to the scattering by those whistlers of multiple, separately located precipitation bursts. Such bursts would result in multiple ionospheric disturbances, two of which might perturb the amplitude of a subionospheric signal with opposite polarity. The peculiar slow-onset and "overshoot" signatures of April 16, 1990 could thus result from the superposition of two competing signal perturbations caused by simultaneous but spatially separate ionospheric disturbances, while the downgoing signatures, with more typical onset behavior, result from a single ionospheric disturbance.

We test this hypothesis by closely comparing the upgoing and downgoing signatures. If the slow-onset upgoing signature represents competing "up" and "down" signal perturbations and the downgoing signature represents only the "down" perturbation component, we can reconstruct an approximate "up" perturbation component by subtraction. As shown in Figure 10, the subtraction of event *f* from event *a* suggests an "up" perturbation component

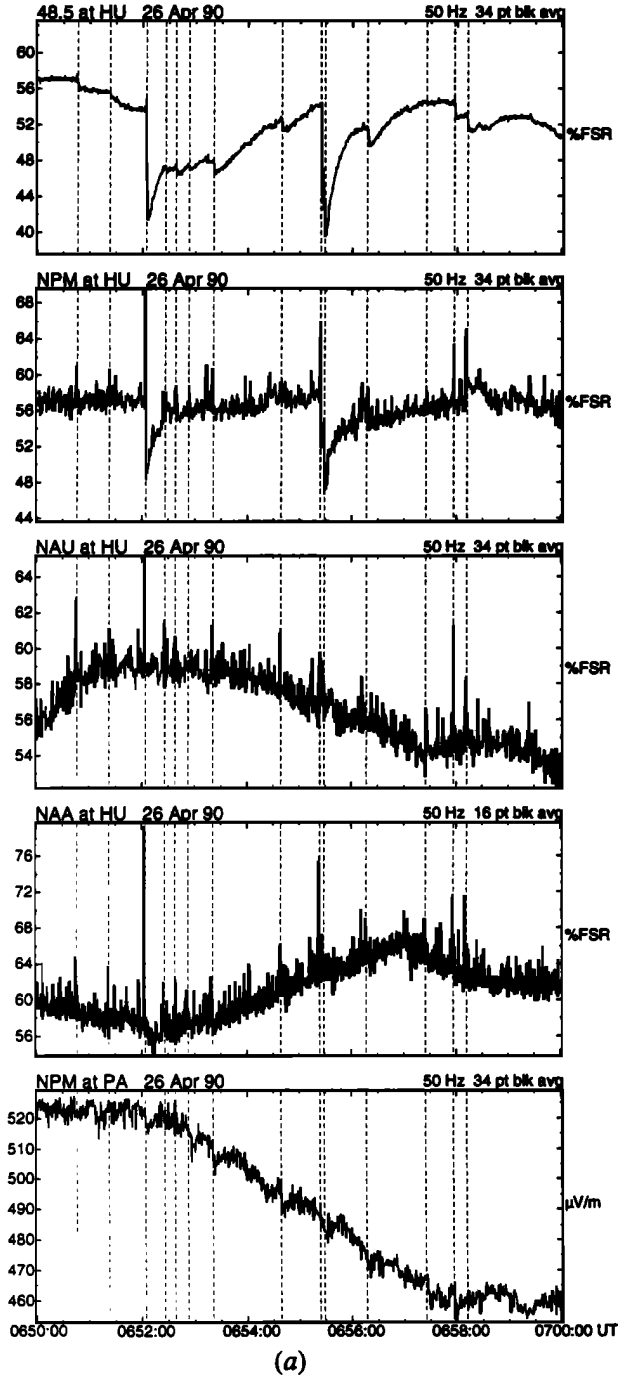

(a)

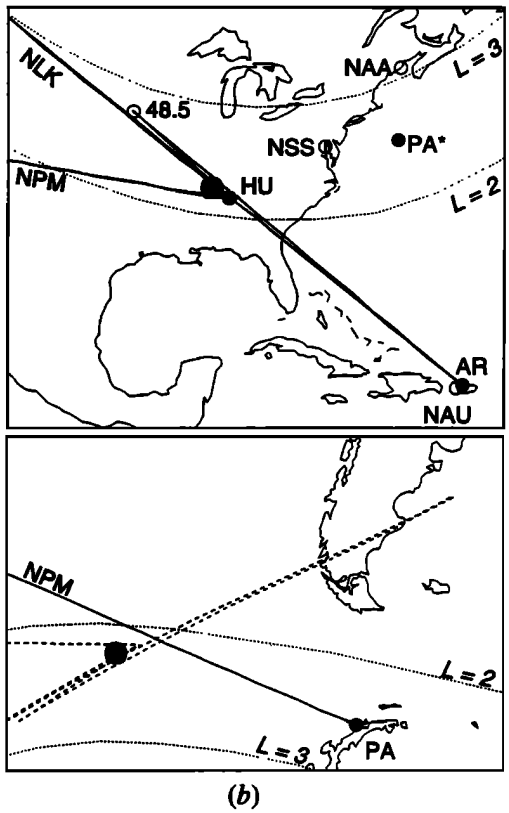

(b)

Fig. 5. (*a*) Ten minutes of narrow-band signal amplitudes on April 26, 1990. No data were available from LM. Of all monitored signal paths, only 48.5–HU, NPM–HU, NLK–HU, 48.5–AR, and NLK–AR were clearly perturbed. The first two of these are shown at top. Narrow-band causative sferics are strong on NPM–HU, NAU–HU, and NAA–HU. Dashed vertical lines indicate the onsets of fourteen 48.5–HU signal perturbations. Using these as a reference, very slight (<0.1 dB) simultaneous perturbations of NPM–PA become noticeable. (*b*) The paths of all perturbed signals are drawn as solid lines. The location of the Palmer Station conjugate (PA*) and of the southern hemisphere conjugates of the perturbed signal paths (dashed lines) are shown for reference. The configuration of perturbed signal paths suggests that the ionosphere was disturbed slightly to the northwest of HU. A possible pair of conjugate disturbance zones ~200 km in diameter is represented as a large black dot in each panel.

for event *a* which compares well with more characteristic signatures such as those observed on NSS–PA.

By the same token, the "overshoot" signatures could be decomposed into "up" and "down" perturbation components of unequal magnitudes, with the "down" component stronger at first but soon overwhelmed by the longer recovery time of the "up" component. In the general case one would expect to see a continuum of signatures, ranging from upgoing to overshoot to downgoing, depending on the relative strength of the "up" and "down" perturbation components. If a duct-disturbance association holds, the relative strength of the perturbation components would in turn depend on the relative strength of the associated whistler components.

To evaluate the dependence of signal perturbation signature on relative whistler component strengths, we must first identify the associated whistler components. This task is complicated by the presence of at least eight clear components in each multipath whistler (Figure 9) which are partly obscured by several additional and less distinct components. A study of the timing, arrival azimuth, and intensity of the identified whistler components leads us to associate the γ whistler component with the "up" perturbation component, and, with less certainty, the ϵ whistler component with the "down" perturbation component. While the intensity of the γ whistler component corresponds well to the observed magnitude of the upgoing signal perturbations, we associate the ϵ component with the downgoing perturbations only on the basis of timing and uncertain evidence that its arrival azimuth at Palmer Station matches that of the NPM signal within ±30°.

Figure 11 shows a progression of the 13 perturbation signatures ordered by the relative magnitude of the γ and ϵ whistler components. Despite the uncertainty in the identification of the associated whistler components, the signatures show a distinct trend from upgoing to overshoot to downgoing (the ordering was also performed using the magnitudes of the β and δ components in place of the ϵ component, but in both those cases the progression was marginally less clear than when using the ϵ component). This

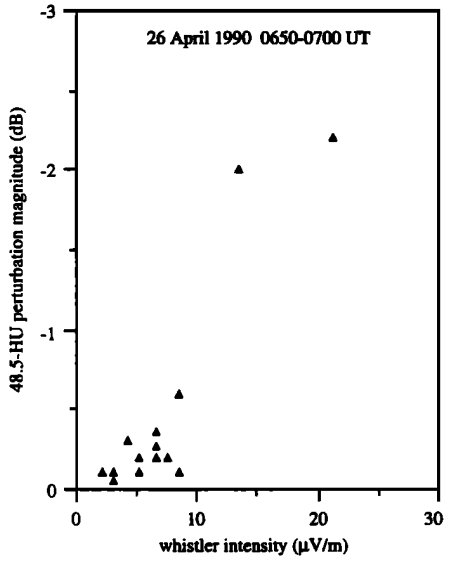

Fig. 6. The intensities of the whistlers observed at Palmer Station on April 26, 1990 compared with the magnitudes of associated perturbations of the 48.5–HU signal. Fourteen perturbations were recorded between 0650 and 0700 UT. A positive correlation is consistent with the scattering and precipitation of electrons by the observed whistlers during ducted propagation. Perturbation magnitude measurements have an error of ±0.1 dB, and whistler intensity measurements have an error of ±25%.

result is consistent with a one-to-one relationship between multiple ionospheric disturbances and the components of multipath ducted whistlers.

The multiple disturbance hypothesis is also supported by the multiplicity of signal paths, nine in all, perturbed simultaneously in both hemispheres. If we assume that individual disturbances are centered within 200 km of perturbed signal paths [*Inan et al.*, 1990; *Poulsen et al.*, 1990] and are located at $1.8 \leq L \leq 2.2$ (the range corresponding to the strongest whistler components observed), at least three disturbances in the south and two in the north are necessary to explain the perturbed signal path configuration (Figure 7*b*). If instead the signal perturbations were all caused by a single, centrally located ionospheric disturbance and its conjugate, such a disturbance would have had to perturb signals whose paths lay 600 km from its center. While such effects have been proposed by *Dowden and Adams* [1990] as a result of deeply penetrating, almost discontinuous disturbances ("stalactites"), the onset and recovery behavior in this case appears to be more consistent with multiple smaller disturbances. Also, given the link between individual disturbances and whistler components just discussed, the presence of several conjugate disturbance pairs would be consistent with the large number of whistler components observed.

The inferred "up" and "down" perturbation components exhibit markedly different recovery times of ~100 s and ~10 s, respectively; of course, without some disparity in recovery, the signatures would either appear normal or be invisible altogether. The fast-recovering "down" signatures appear to be associated with whistler component ϵ, which propagated at $L \simeq 2.2$, while the slow-recovering "up" signatures appear to be associated with component γ, propagating at $L \simeq 1.9$. The disparity in recovery times at the different L shells is in the opposite sense to predictions for the variation of recovery rate with L based on the energy spectrum and depth of ionospheric penetration of whistler-induced precipitation bursts [*Inan et al.*, 1988*a*]; however, those predictions assumed a constant and uniform whistler spectral density. The ϵ component is stronger than the γ component below 1.5 kHz, a frequency which corresponds at these L values to equatorial resonant loss-cone electron energies of about 500 keV; therefore, the ϵ component may be associated with more precipitation of >500-keV electrons than the γ component. The faster recovery signatures associated with the ϵ component may thus be related to the faster effective recombination rates expected at the mesospheric altitudes ionized by such high-energy particles [*Inan et al.*, 1988*a*]. Additional factors, such as the duct shape or anomalies in radiation belt electron populations, may also play a role in precipitation burst energy spectra and resulting recovery signatures.

During the 11-min period shown in Figure 7*a*, a total of 20 multipath whistlers were observed whose strongest components exceeded a threshold of ~2 μV/m; however, even though all 20 whistlers exhibited similar multipath and dispersion characteristics, only 13 were associated with signal perturbations. The seven unassociated whistlers were consistently weak (none exceeded 19 μV/m, 6 dB weaker than the weakest of the associated whistlers (event *i*)), but even so, they were stronger than those of the April 26, 1990 case discussed earlier for which associated signal perturbations were observed. The lack of signal perturbations for the weaker whistlers on April 16 may indicate that the precipitation regions were located far enough from the monitored signal paths that only the stronger whistlers could induce enough precipitation to detectably perturb a signal. This interpretation is consistent with the presence of upgoing perturbations on a majority of the nine perturbed signals, since upgoing perturbations of a signal were attributed by *Poulsen et al.* [1990] to disturbances located 100–200 km off the signal path (Figure 3). Some of the observed perturbations may also have been associated with whistler components other than the strongest; the intensities of these weaker components would more closely compare with those of the weak whistlers observed on April 26. Finally, the April 16 whistlers could have exited their ducts closer to Palmer Station than those on April 26, which would be consistent with the higher range of whistler intensities observed.

We have interpreted the "overshoot" effect as a result of multiple ionospheric disturbances, but the converse would not be strictly true: multiple disturbances would not necessarily always result in overshoot signal perturbations. To cause an overshoot effect, there must be at least two disturbances close enough to a signal path to perturb it; the disturbances must be located so that one will perturb the signal amplitude upward and the other will perturb it downward [*Poulsen et al.*, 1990]; and the recovery rates of the "component" perturbations must be different. Even if multiple disturbances are the rule rather than the exception, as the evidence in this paper suggests, these conditions for "overshoot" signatures would still be only rarely fulfilled. This evaluation is consistent with the paucity of overshoot signatures in our data at large, comprising less than 1% of all perturbations observed.

5. Arrival Azimuths of Associated Whistlers

The temporal associations between ducted whistlers and signal perturbations that we have discussed so far not only support a cause-effect relationship between the two, but imply that the phenomenon is global and widespread. Precipitation zones may exist at the northern and southern feet of every excited whistler duct. To explore this possibility more deeply, we now turn to the spatial correspondence between ducted whistlers and signal perturbations, which we investigate by looking for an association between duct exit locations and the locations of ionospheric disturbances. Such a comparison was first performed in a preliminary

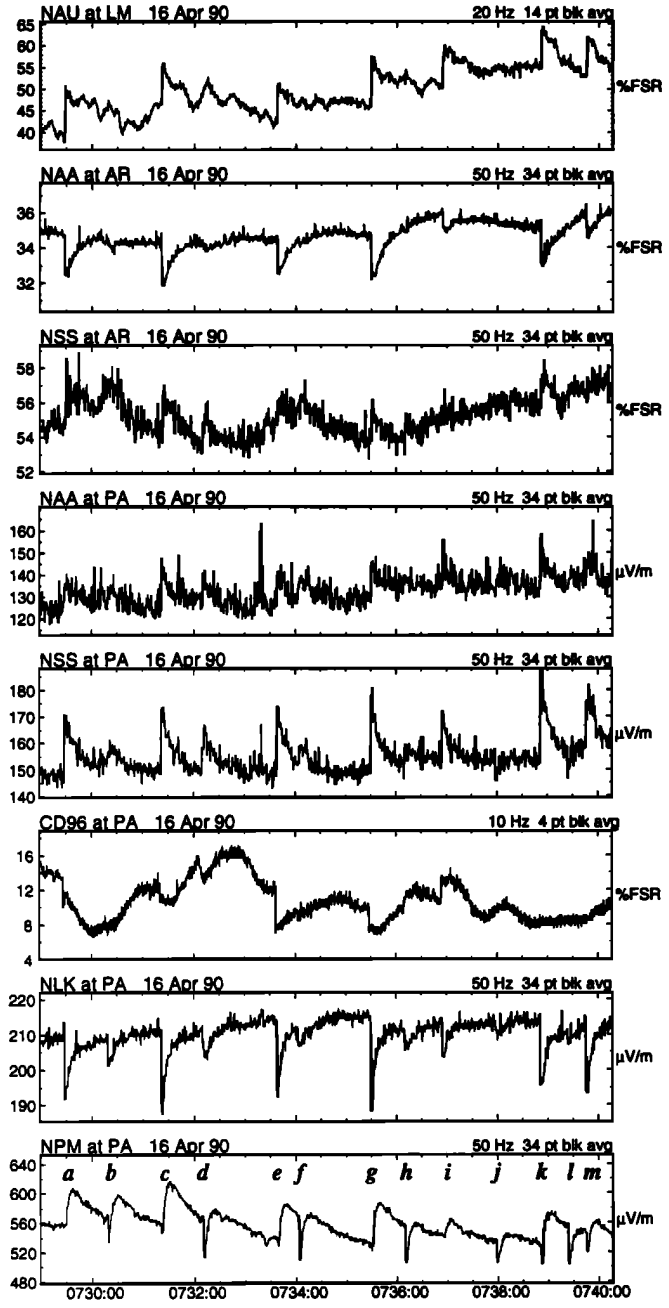

(a)

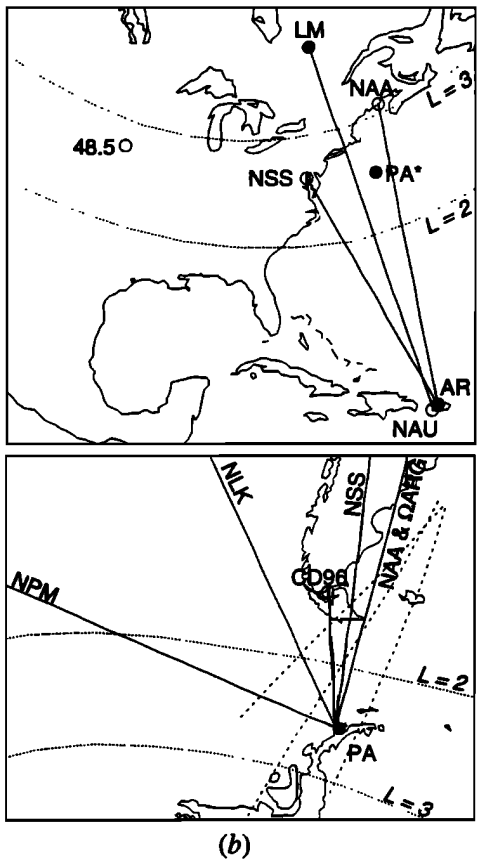

(b)

Fig. 7. (*a*) An 11-min period of simultaneous signal perturbations on eight signal paths observed on April 16, 1990 (Omega Argentina at PA was also perturbed but is not shown). The 13 events detected on NPM–PA during the period are marked *a* through *m* for identification. The unusually slow onset behavior and occasional initial downward excursions ("overshoots") of the upgoing events on NPM–PA are interpreted in the text as resulting from multiple ionospheric disturbances near the NPM–PA signal. (*b*) The format of the map is identical to that of Figure 5*b*. HU is not shown because no data were available from that site.

survey by *Carpenter and LaBelle* [1982], who found a statistical correlation between the arrival azimuths of ducted whistlers at Palmer Station and the arrival azimuths of subionospheric signals which were perturbed during the same period; however, the scope of this work was limited at the time by the direction-finding method available and by the lack of northern hemisphere signal perturbation data.

Electron Precipitation Near Huntsville

Signal perturbations recorded on April 19, 1990, illustrated in Figure 12, indicate the presence of an ionospheric disturbance in the vicinity of HU. During the 10-min period shown, HU observed simultaneous perturbations on all signals except NAU, while at Palmer Station NPM–PA was the only perturbed path. Data from AR and LM were unavailable. The simultaneous perturbation of NPM–PA is consistent with a precipitation-induced ionospheric disturbance conjugate to HU [*Burgess and Inan*, 1990], although the lack of perturbations on NAU–HU may indicate that the northern hemisphere disturbance was slightly to the north of HU.

To facilitate the comparison of the signal perturbations with whistlers, perturbations larger than a threshold of 0.2 dB on NPM–HU or 0.1 dB on NPM–PA are marked *A* through *U*. The poorer detectability threshold on NPM–HU was due to atmospheric noise. Twenty-two events were observed on NPM–HU, of which 16 were observed nearby simultaneously on the more weakly perturbed NPM–PA (the six events not detected on NPM–PA corresponded to the weakest 6 events of the 22 measured on NPM–HU, and may simply have been below the Palmer Station receiver's noise floor). No broadband data were available for the event marked with an asterisk, so this event is excluded from further discussion. Of the 21 remaining marked events, all corresponded to whistlers observed at Palmer Station. At Palmer Station a total of 23 whistlers stronger than 2 μV/m were recorded during this period, which leaves two whistlers unassociated with any detected signal perturbation.

The arrival azimuths at Palmer Station of all 23 multipath whistlers, calculated including all components in each whistler, are shown in Figure 13. The mean arrival azimuth of the 21

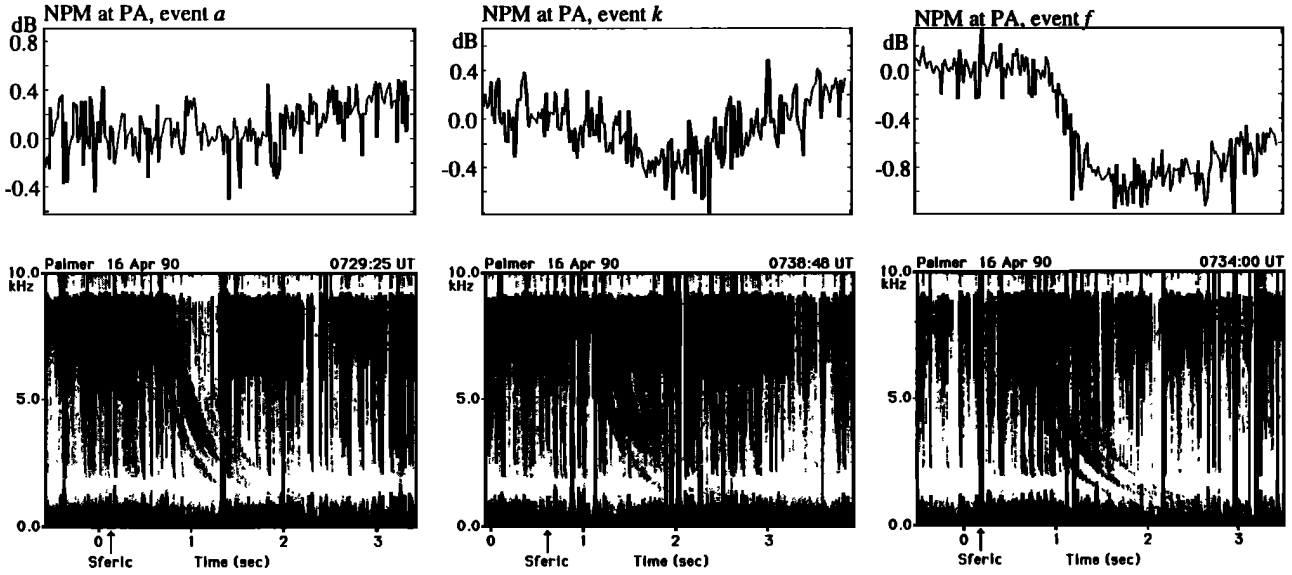

Fig. 8. Examples of the time association between whistlers and NPM–PA signal perturbations for 3 of the 13 events marked in Figure 7, representing slow-onset upgoing (event *a*), overshoot upgoing (event *k*), and normal downgoing (event *f*) perturbation signatures. Analysis of these and the other events in Figure 7*a* indicates a link between perturbation signature and the relative strength of associated whistler components. The 0-dB reference corresponds to the ambient preperturbation signal level in each case. The spectrograms display a 30-dB dynamic range, with maximum intensity (black) representing signals $\geq 95\mu$V/m, and with a frequency resolution (Δf) of 61 Hz.

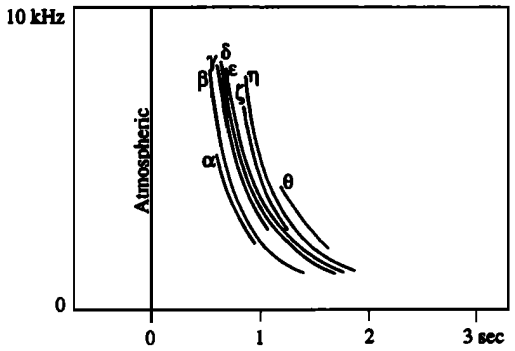

Fig. 9. A schematic identification of whistler components in Figure 8. The intensity of the γ component in particular appears to correspond to the upgoing magnitude of the associated NPM–PA signal perturbations shown in Figure 8.

perturbation-associated whistlers, determined by averaging the peaks of the azimuth main lobes shown in Figure 13, is 278°. This value matches the azimuths of NPM (276°) and of the conjugate of HU (273°) well within the ±15° absolute azimuth error. The *L* shell of the first component of the associated whistlers was ~2.0, which compares well with that of HU ($L = 2.13$) and resolves the 180° arrival azimuth ambiguity in favor of the northwest. Of the two whistlers unassociated with any detected signal perturbation, one was the second weakest whistler observed (2 μV/m) and the other, though much stronger (15 μV/m), arrived from an azimuth of 345° (regrettably, LU14, which arrives at Palmer Station with an azimuth of 346°, was off the air during this period). Figure 14 compares the second unassociated whistler with the whistler for event *L*.

The correspondence between the inferred locations of ducts and disturbances on April 19, 1990 is consistent with conjugate precipitation by ducted whistlers. The fact that the only two unassociated whistlers observed were weak or from a region unmonitored by signal paths suggests that, had those whistlers also induced precipitation which caused ionospheric disturbances, such disturbances would not have been detected.

The clustering of the multipath whistlers' arrival azimuths in the direction of the HU conjugate suggests the presence of multiple ducts, and therefore multiple disturbances, in the vicinity of HU. The fact that not all paths at HU were perturbed by the same relative magnitudes in each event, as seen especially for events *C*, *H*, and *S* on the 485–HU, NSS–HU, and NPM–HU signals in Figure 12, is consistent with the disturbance of multiple ionospheric regions near HU by different relative amounts on each occasion. This interpretation is reinforced by the difficulty in explaining these changing relative signal perturbation magnitudes in terms of a sequence of disturbances occurring in a single location. In this case, the varying relative signal perturbation magnitudes from one event to the next would mean that changes in the structure of each individual ionospheric disturbance were affecting the waveguide response of each perturbed signal differently. It seems unlikely, however, that precipitation bursts associated with the same duct, and therefore presumably with similar energy distributions, would induce profiles of secondary ionization which varied sufficiently from event to event to affect waveguide responses differently. Note that the 16 perturbations observed simultaneously on NPM–HU and NPM–PA exhibited uncannily constant relative magnitude (Figure 15) despite their resulting from disturbances inferred to be in opposite hemispheres.

The onset behavior of conjugate signal perturbations on April 19, 1990, is compared with LEP theory in section 6.

Whistler Component Azimuths

Arrival azimuth measurements on individual components of multipath whistlers can shed light on the relationship between multipath whistlers and multiple ionospheric disturbances. If multiple, simultaneous disturbances correspond one-to-one with the ducts excited by a multipath whistler, and those disturbances perturb subionospheric signals, then there should be at least one duct exit near every perturbed signal path, probably within 200 km (Figure 3).

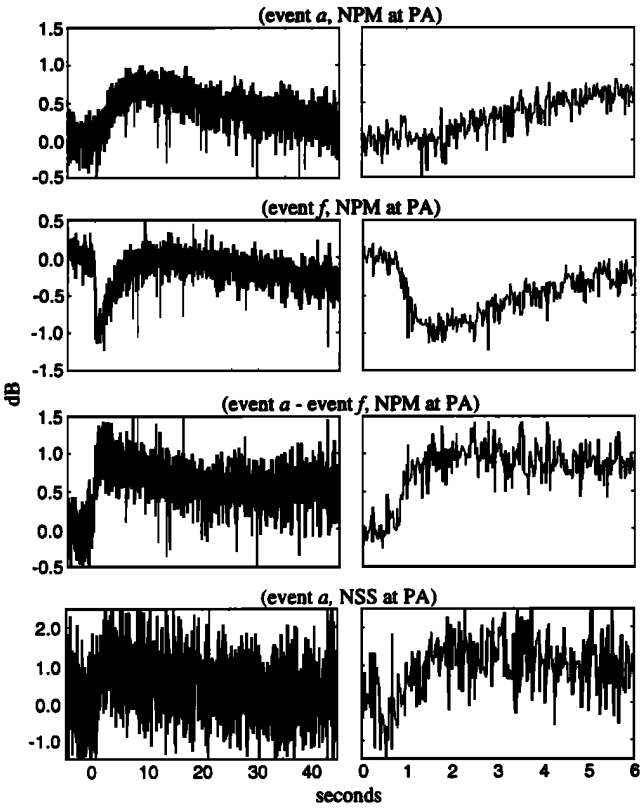

Fig. 10. Reconstructing an approximate "up" perturbation component. The slow-onset upgoing signal perturbation signatures shown in Figure 7 appear to have resulted from the superposition of a slow-recovery upgoing perturbation and a fast-recovery downgoing perturbation. To investigate this possibility, we estimate an upgoing "component" perturbation for event *a* by subtracting event *f*, a typical downgoing event, from event *a*. The result suggests an upgoing component which compares well with more normal onset behavior, such as that exhibited by NSS–PA. In all panels, $t = 0$ corresponds to the time of the causative sferic. The 0-dB reference corresponds to the ambient preperturbation signal level in each case.

Figure 16 shows the simultaneous perturbation of four signal paths observed at PA and one at AR. Other signals monitored at the two sites were not detectably perturbed, and no data were available from HU or LM. Twenty-six perturbations greater than 0.1 dB were observed on NPM–PA during the half-hour shown. All 26 events were associated with multipath whistlers with maximum intensities ranging from 5 to 53 μV/m. It is difficult to postulate a single conjugate pair of spatially extensive disturbances to explain the observations because several other signals propagating within both conjugate regions were not detectably perturbed. The observations thus appear to be more consistent with multiple smaller disturbances.

Arrival azimuths measured for the components of the associated whistlers are consistent with a duct-disturbance association. Figure 17 shows an example of an associated whistler, in which three major components are identified as α, β, and γ. These three components were strong and isolated enough for their azimuths to be analyzed individually, with the results shown in Figure 18. The α component arrived at Palmer Station from the same direction as NSS and LU14, two of the perturbed signals. The β component arrived from the same direction as NLK, which was also perturbed.

When L shells of α, β, and γ are also considered, the resulting position "fixes" do not indicate ducts on or near NPM–PA or NSS–AR, both of which were strongly perturbed. As we have

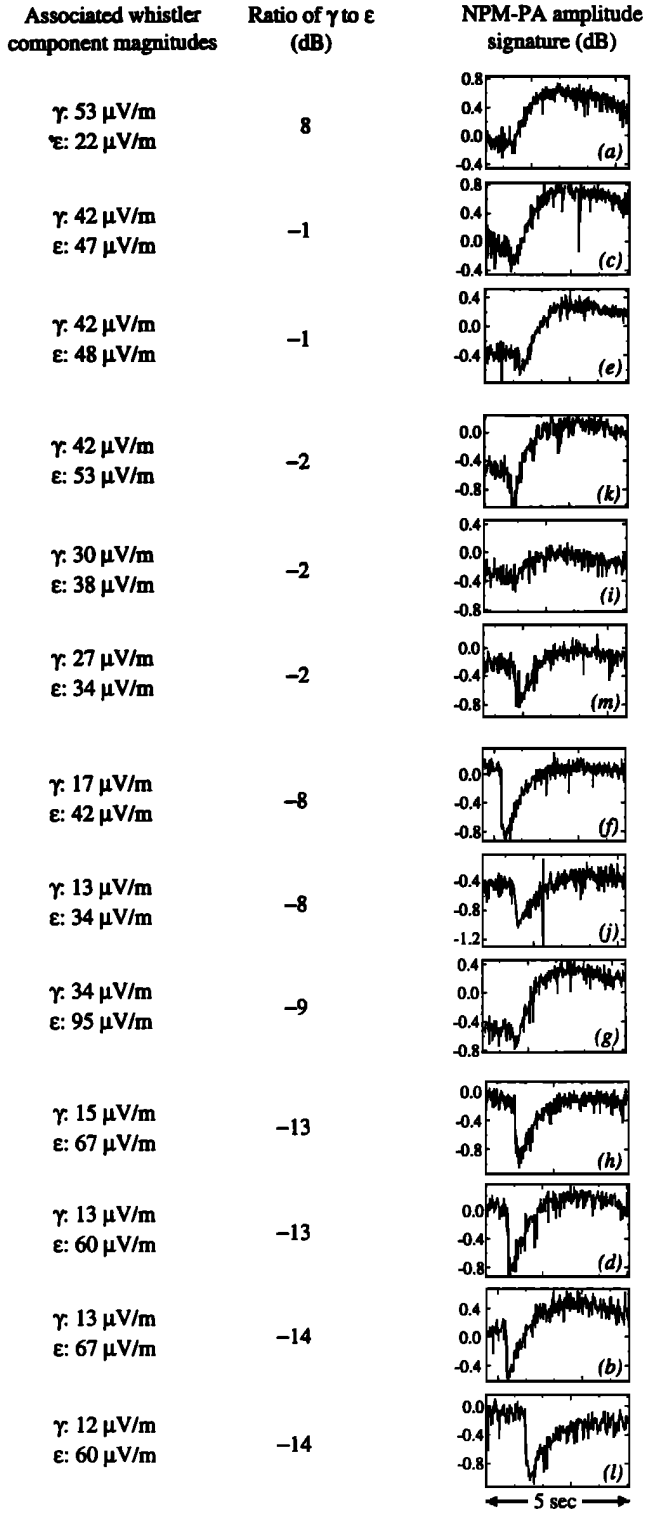

Fig. 11. The NPM–PA signatures identified in Figure 7 are ordered by the relative magnitude of the γ and ϵ components of the associated whistlers. The signature progression, from upgoing to overshoot to downgoing, is consistent with a cause-effect association between the intensity of individual ducted whistler components and the magnitude of individual ionospheric disturbances. The aberrant placement of signature *g*, whose associated whistler possessed an unusually intense ϵ component, suggests that the relationship between component intensity and disturbance magnitude is not linear for strong events, possibly indicating a "saturation" effect for LEP-induced ionospheric disturbances. Whistler component magnitude measurements have an error of ±25%. In all cases 0 dB represents 560 μV/m narrow-band signal strength of NPM–PA.

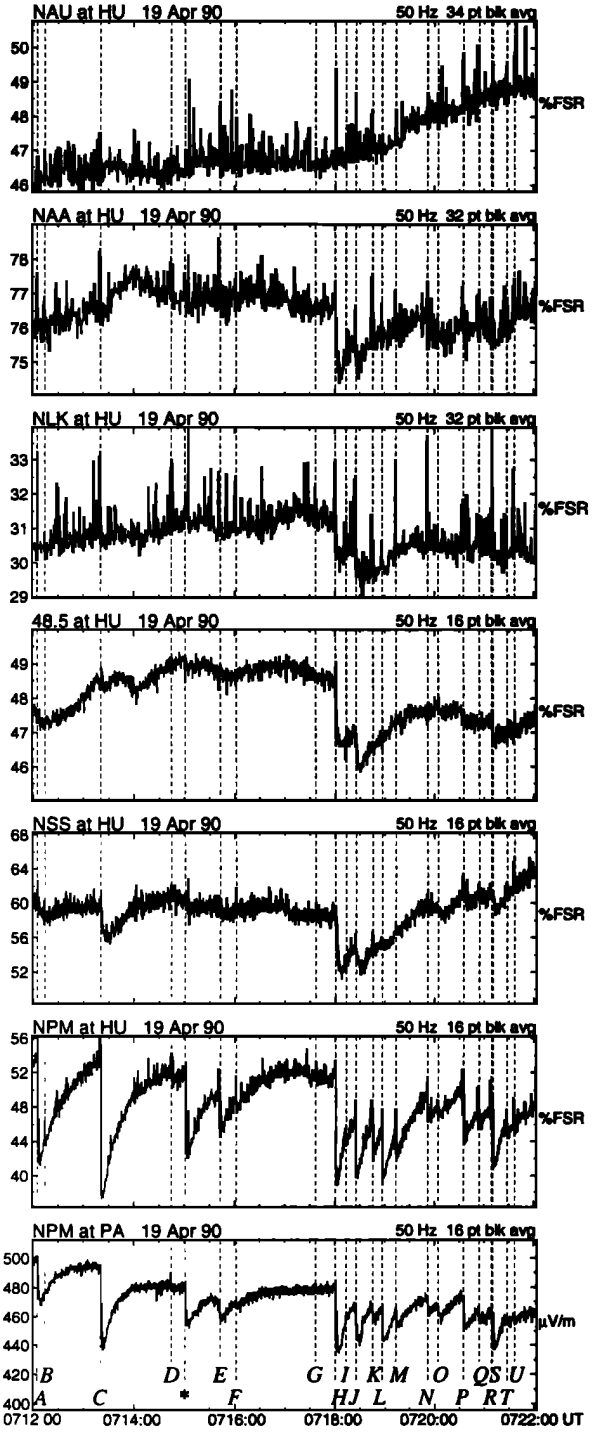

(a)

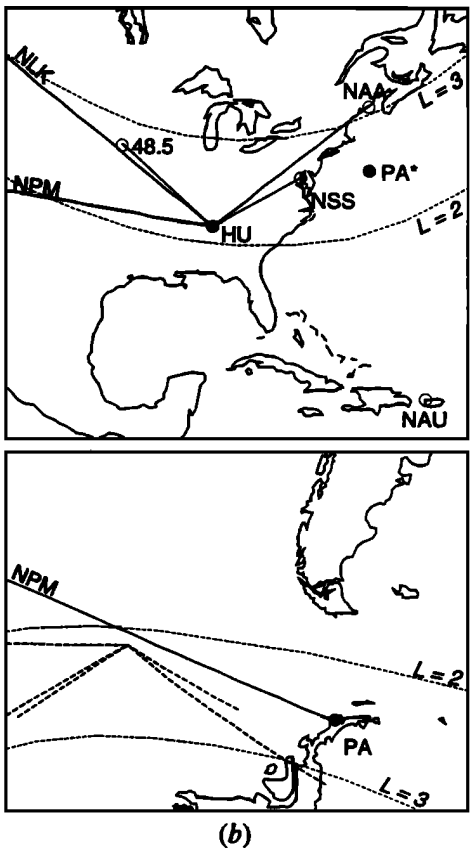

(b)

Fig. 12. (*a*) A 10-min period of simultaneous signal perturbations on six signal paths observed on April 19, 1990 (NAU–HU was not perturbed but is shown at top for reference). Dashed vertical lines indicate the onset times for 22 perturbations observed on NPM–HU, 16 of which were nearly simultaneous (±1 s) with perturbations of NPM–PA. These events are marked *A* through *U* (no broadband data were available for the event marked with an asterisk). (*b*) The format of the map is identical to that of Figure 5*b*. AR and LM are not shown because no data were available from those sites. The configuration of perturbed signal paths suggests the presence of one or more ionospheric disturbances in the vicinity of HU.

already seen, however, NPM–PA perturbations can be associated with extremely weak whistlers. Such whistlers could easily have been overwhelmed in the azimuth analysis by noise or by stronger whistler components from other directions. The lack of an identifiable duct associated with NSS–AR may be due to a similar cause.

The duct associated with the β component appears to have been within ± 0.1 L shell of Palmer Station. The lack of detectable perturbations on three of the seven signals monitored at Palmer Station, despite the apparent proximity of the β duct and its inferred associated disturbance, is not inconsistent with *Poulsen et al.*'s [1993] subionospheric VLF wave scattering model. This model suggests that wave scattering from whistler-induced ionospheric disturbances is mostly into a near-forward direction. Thus, if the disturbance was located on the NLK–PA path, as implied by the arrival azimuth of the associated whistler, considerable sideways scattering by the disturbance of any other monitored signals, such as NAA for example, would be required to result in detectable perturbations of those signals at Palmer Station.

6. Signal Perturbation Onsets and LEP Theory

The possibility that every ducted whistler component can induce precipitation is consistent with the theory of gyroresonant interaction between ducted whistlers and radiation belt electrons developed by *Chang and Inan* [1985]. No theoretical evidence was found which suggests any abrupt thresholds in the ability of ducted whistlers to scatter electrons. However, while the theory has been successfully applied to precipitation bursts observed in situ [*Inan et al.*, 1989], lack of high-time resolution narrowband recordings has prevented all but limited comparison of theory with ground-based signal perturbation data [*Carpenter et al.*, 1984; *Inan et al.*, 1985*a*].

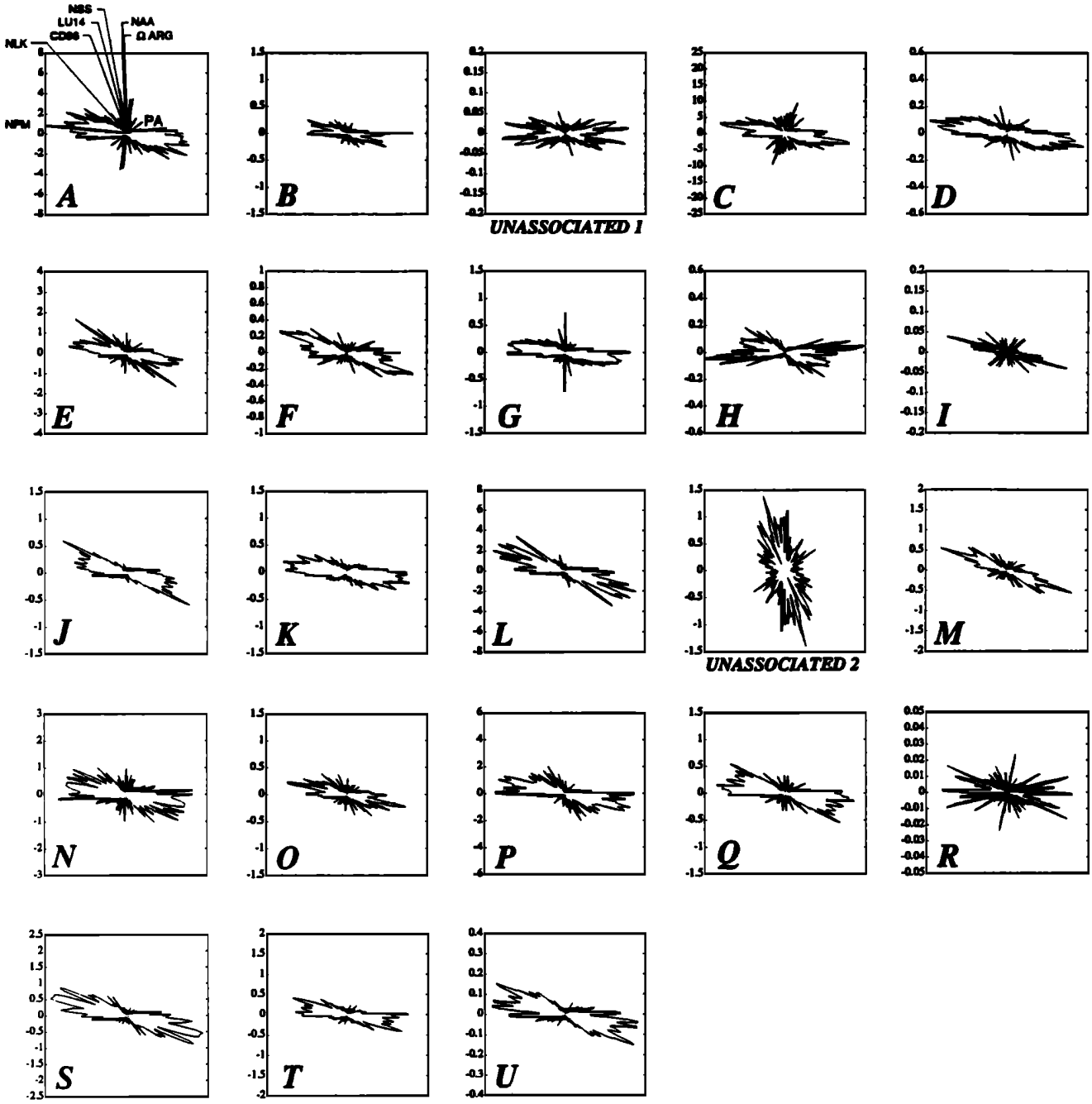

Fig. 13. The arrival azimuths of the 23 multipath whistlers observed at PA between 0712 and 0722 UT on April 19, 1990. The 21 lettered plots correspond to whistlers associated with the signal perturbations shown in Figure 12. The remaining two whistlers were not associated with detected signal perturbations. All whistlers arrived from lower L shells than that of PA ($L \simeq 2.4$) which resolves the 180° ambiguity in each plot in favor of the northwestern lobe. The average main lobe peak azimuth for the associated whistlers was 278°, which matches the azimuth of NPM (276°) and of the conjugate of HU (273°) within the ±15° absolute azimuth error. Of the unassociated whistlers, one was the second weakest observed and the other, though relatively strong, arrived from a different direction. The plots were generated by sampling the arrival azimuth of each whistler along its curve in the frequency-time plane, and weighting each azimuth sample by the corresponding intensity of the whistler. All whistler components were included in each analysis. The plots are oriented with the top of the page representing geographic north. The relative amplitude scales are only approximately uniform due to the weighting method used.

To determine if signal perturbations are consistent with the *Chang and Inan* [1985] model of electron scattering and precipitation by ducted whistlers, we compare the timing of predicted conjugate precipitation bursts with observed perturbation onsets in the northern and southern hemispheres. Examples of conjugate perturbation onsets during a half-hour period on April 19, 1990 and a 4-min period on March 21, 1989 are shown in Figure 19. Six events from April 19 and two events from March 21 were selected for analysis using clarity of onset and lack of interfering atmospheric noise as criteria. The events were then superposed to further improve onset definition.

For a superposition time reference, we used the estimated time that the causative sferic first entered a magnetospheric duct. To find this time, we assumed that the source lightning occurred

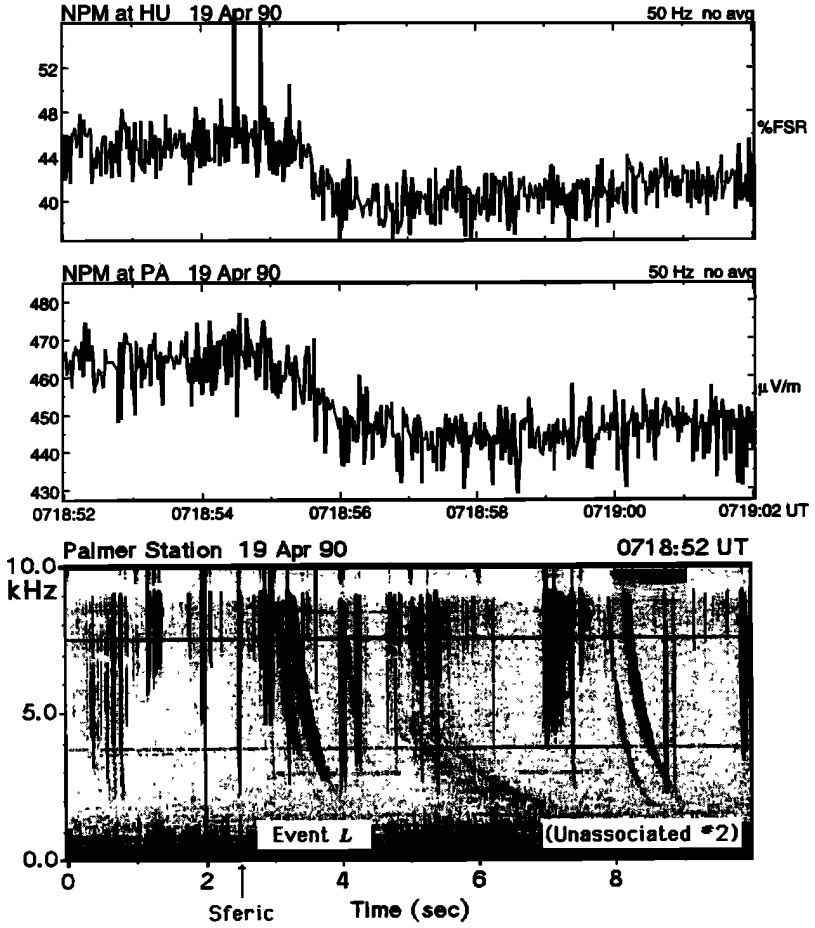

Fig. 14. Two signal perturbations and the whistler associated with event L are compared with the lack of perturbations and the second unassociated whistler from the period shown in Figure 12.

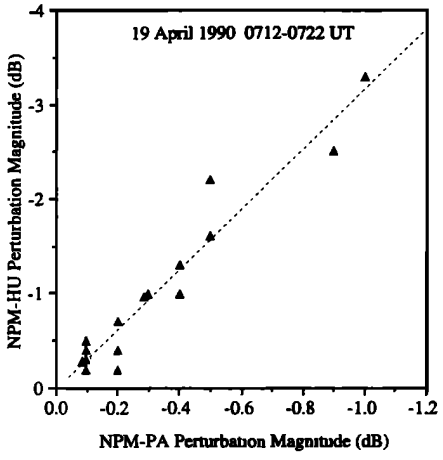

Fig. 15. The relative magnitude of 16 nearly simultaneous perturbations observed on NPM–HU and NPM–PA on April 19, 1990 was almost constant, consistent with twin ionospheric disturbances, one in each hemisphere, caused by conjugate precipitation bursts with similar energy spectra. The disturbances are unlikely to have been in the vicinity of the NPM transmitter because simultaneous perturbations were observed on other signals arriving at HU (see Figure 12). The least squares fit shown has a slope of 3.2 to one, a y intercept of -0.02 dB, and represents a correlation coefficient of 0.96. Perturbation measurements have an error of ±0.1 dB.

over the eastern United States, an assumption supported by strong narrow-band causative sferics at HU on April 19, 1990, and by lightning detection data on March 21, 1989 [*Burgess and Inan*, 1990]. We assumed further that the propagation delay between the location of the lightning flash and the region where the resulting sferic coupled into the magnetosphere is negligible. These assumptions allow us to estimate initial magnetospheric entry time as the time of the associated whistler causative sferic recorded at Palmer Station minus 39 ± 5 ms of propagation delay from the flash location to Palmer Station.

The initial electron precipitation pulse in the northern hemisphere (pulse I) was scaled in time from a prediction for $L = 2$ and $N_{eq} = 1300$ el cm^{-3}, made using a comprehensive treatment of scattering by ducted whistlers, presented in Figure 11*b* of *Chang and Inan* [1985]. Time scaling of the original pulse was necessary to correct for observed values of associated whistler L and N_{eq}, and was performed based on the difference in peak flux arrival time (t_p) as predicted by a simple model of equatorial electron gyroresonance with a reference wave at a given frequency f_{ref}. Whistler mode propagation delay at $f = f_{ref}$ was modeled as a function of L and N_{eq} using the dispersion predicted by *Daniell* [1986*b*], assuming a ratio of whistler nose frequency to equatorial gyrofrequency (Λ_n) as given for a diffusive equilibrium electron distribution by *Bernard* [1973]. We found that choosing $f_{ref} = 6.3$ kHz was all that was necessary to calibrate the model to within ±30 ms of the t_p curve for $1.8 \leq L \leq 2.4$ and $N_{eq} = 8128 \times 10^{-0.359L}$ el cm^{-3} given by *Chang and Inan* [1985, Figure 8]. We then used the model with measured values of whistler L and N_{eq} to estimate t_p and to time scale the original precipitation pulse for the observed cases.

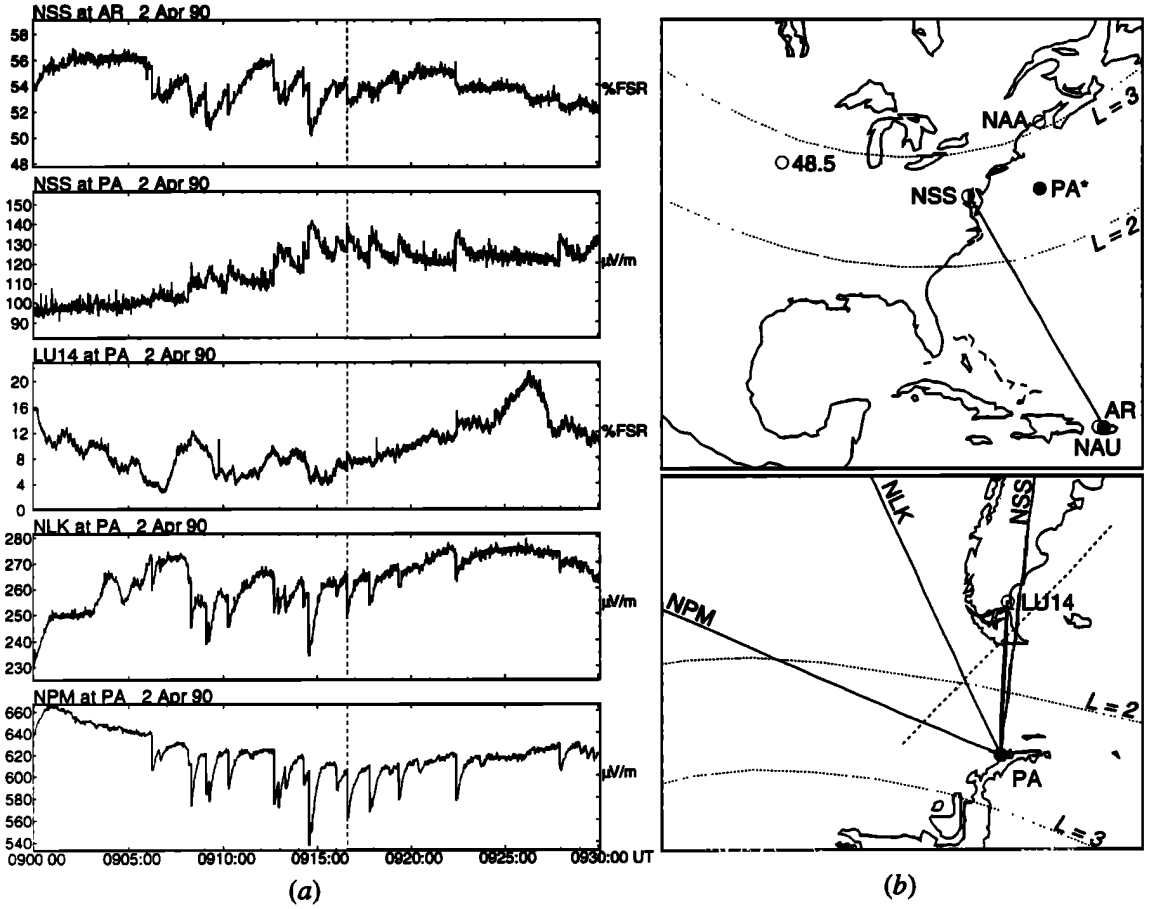

Fig. 16. (*a*) Thirty minutes of narrow-band signal amplitudes recorded on April 2, 1990. The dashed vertical line indicates the onset of a perturbation event to be examined in greater detail. No other observed signal paths at AR or PA were perturbed, and no data were available from HU or LM. (*b*) The format of the map is identical to that of Figure 5*b*.

The first precipitation pulse to strike the southern hemisphere, which is the second pulse to approach the Earth (pulse II), was time-scaled from *Chang and Inan* [1985, Figure 11*d*], using the same simple model for t_p except with the addition of a one-hop bounce time for loss-cone electrons that would resonate at the equator with 6.3 kHz. This choice of bounce time is only a ballpark estimate for the range of electron energies that would be involved in the precipitation burst, but it is adequate at relativistic energies where velocity no longer varies as the square root of energy; for example, bounce periods for electron energies of 50 and 500 keV at a given L shell and pitch angle differ by only about a factor of 2. Bounce periods of 6.3 kHz-resonant loss-cone electrons are 0.33 s (128 keV, $L = 2.05$) and 0.47 s (64 keV, $L = 2.23$) for the April 19 and March 21 cases, respectively, shown in Figure 19.

The later precipitation pulses (pulse III in the northern hemisphere and pulse IV in the southern hemisphere) were predicted from pulses I and II by keeping the time delay between pulse beginnings constant, and likewise for pulse endings. No modification was made to the original amplitudes of pulses I and II, which *Chang and Inan* [1985] calculated assuming 100% mirroring or backscatter and ignoring any loss-cone asymmetry. The amplitudes for pulses III and IV were generated from pulses I and II by keeping the peak amplitude ratio of a given pulse to the previous pulse constant.

In the April 19 case, experiment agrees well with theory. The northern hemisphere is perturbed earlier than the southern hemisphere, as expected. The predicted onset delay does appear perhaps 0.2 s too short, but this may be due to selection of the leading whistler component to provide L and N_{eq}. As discussed earlier, several whistler components were observed, and a later one may have been responsible for the disturbances which perturbed NPM–HU and NPM–PA. If so, the delays associated with a later component would reduce the discrepancy in the prediction.

The March 21 data also appear to agree well with predictions, with one exception: one detects no signal perturbation in association with pulse I. The southern hemisphere is perturbed first. As pointed out by *Burgess and Inan* [1990], this effect can be expected at longitudes of the South Atlantic magnetic anomaly, since the population near the northern loss cone is far less than that near the southern loss cone. As demonstrated in Figure 20, it is possible for pulse I to be far weaker than pulse II, in contrast to what is shown in Figure 19, because fewer electrons are available for precipitation into the northern hemisphere [*Inan et al.*, 1988*c*]. That the southern hemisphere was perturbed first on March 21, 1989, but not on April 19, 1990, suggests that the near-loss-cone electron distribution may have been different on the two days.

The onset durations exhibited in both cases extend well beyond the end of the first causative precipitation pulse (pulse I in the northern hemisphere, pulse II in the southern hemisphere). This observation is consistent with the continuing disturbance of the conjugate ionospheric regions by pulses III and IV, and possibly by later pulses as well. Such successive precipitation pulses of diminishing flux have been observed in situ in association with ducted whistlers [*Voss et al.*, 1984].

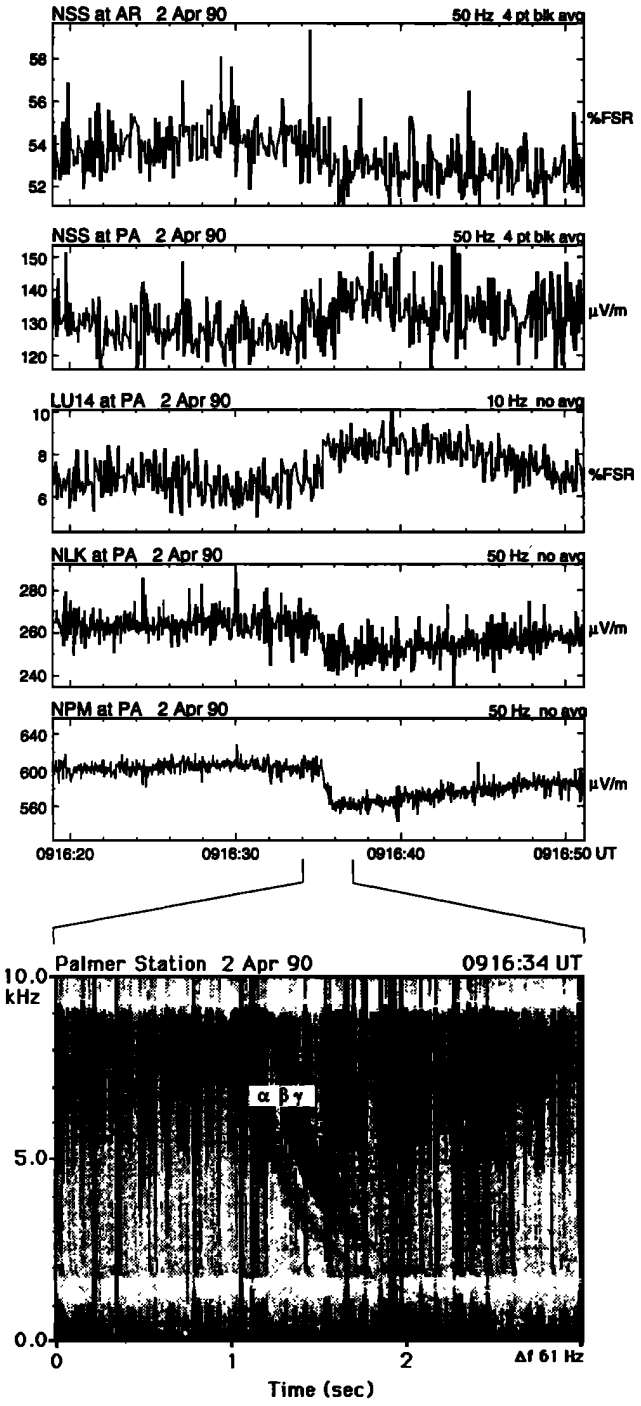

7. THE CONTRIBUTION OF DUCTED WHISTLERS TO RADIATION BELT LOSSES

Assuming that every ducted whistler component precipitates radiation belt electrons, we now estimate a first-order lower bound on the resulting radiation belt losses by comparing ground-observed whistler intensities and occurrence rates with whistler-associated precipitation flux measured in situ. We constrain this analysis to $2 < L < 3$, identified in previous work as the region where most whistler-associated precipitation of >50-keV electrons is expected [*Chang and Inan*, 1985] and appears to occur [*Carpenter and Inan*, 1987].

Equatorial Whistler Intensity

We begin by estimating a representative equatorial wave magnetic field (B_{dw}) for the "average" precipitation-inducing ducted whistler. Since in situ data on ducted whistler intensities are not available, we infer wave intensity in the duct from ground measurements. First, analysis of whistler arrival azimuth and L is used to locate the duct exit point and estimate attenuation resulting from the relative orientation of the receiving antenna. Then, given the distance between the duct exit point and Palmer Station, we apply an Earth-ionosphere waveguide spreading loss of 14 dB in the first 200 km [*Tsuruda et al.*, 1982], followed by waveguide attenuation of 1.6 dB per 100 km up to 1000 km and 0.8 dB per 100 km thereafter, as adapted from *Crary* [1961, Figure 3.9]. After accounting for subionospheric attenuation, we are left with an estimate for the field strength just below the ionosphere in the vicinity of the duct exit point. From this we find the equatorial wave field in the duct using the approach of *Inan et al.* [1984], including lower nighttime ionospheric absorption loss for a 2 kHz signal as given by *Helliwell* [1965, Figure 3-35], changes in the refractive index, and the expansion of duct cross section with decreasing geomagnetic field intensity.

Applying this method to 59 perturbation-associated whistlers recorded on three different days yielded an average duct equatorial field of B_{dw} = 12 pT (Figure 21). Equatorial resonant energies for loss-cone electrons scattered by these whistlers would have ranged from 70 to 700 keV, based on the observed bandwidths of the whistler traces and their associated L and N_{eq} values. For the purpose of discussion we will henceforth take 70 keV as the lower limit of the energy of electrons scattered by ducted whistlers.

Fig. 17. The simultaneous signal perturbation event marked in Figure 16*a* is shown in greater detail and compared with the associated whistler. Although the whistler involved at least seven components, three components were strong and isolated enough to attempt an estimate of their individual arrival azimuths.

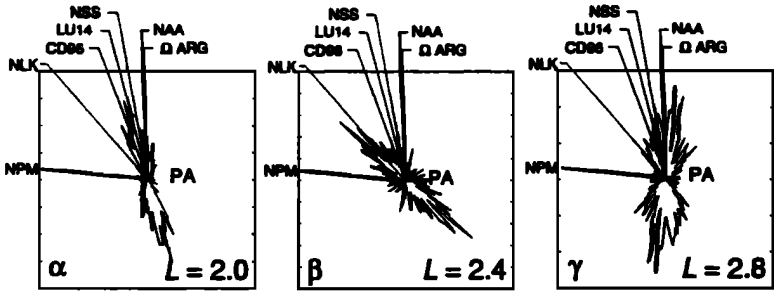

Fig. 18. Arrival azimuths of the three whistler components identified in Figure 17. Component γ arrived from the south of Palmer Station, so the upper lobe of its azimuth plot should be disregarded.

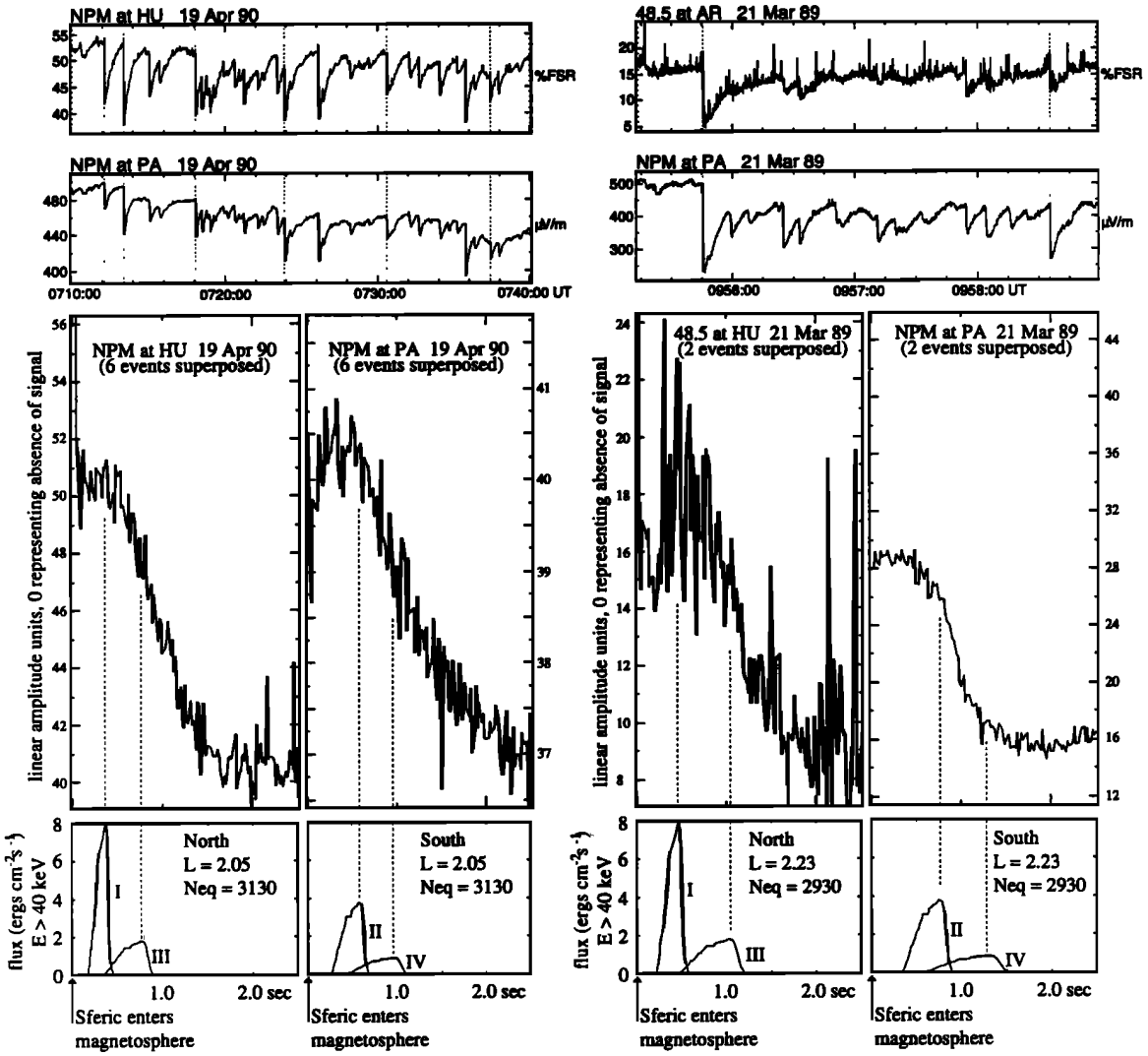

Fig. 19. A comparison of observed signal perturbation onset behavior with the timing of theoretical electron precipitation pulses, which were modeled based on scattering of radiation belt electrons by ducted whistlers. The left panels show the superposition of six signal perturbations selected from a half-hour period on April 19, 1990, and the precipitation pulses predicted using the L shell and N_{eq} corresponding to the associated whistlers. The right panels show a similar analysis of two superposed events from a 4-min period on March 21, 1989. Superposition was carried out using as a $t = 0$ reference the northern hemisphere causative sferic, which is noticeable at the beginning of the northern hemisphere superposition panels. The bouncing pulses are labeled in the order in which they strike the Earth, with I and III striking the northern hemisphere and II and IV striking the southern hemisphere. The perturbation onsets compare well with the timing of the predicted precipitation, except for pulse I on March 21. The lack of a detectable perturbation in association with this pulse is consistent with the relatively small flux on the edge of the northern loss cone in the vicinity of the South Atlantic magnetic anomaly.

Size of the Region Monitored for Whistlers

The next task is to estimate the size of the region for which long-term whistler rate data from a single site might indicate the quantity of associated electron precipitation. Let us say we wish to count at least 95% of precipitation bursts within this region. Of the 59 whistlers just mentioned, 95% (56) corresponded to equatorial fields stronger than 6 pT; we therefore define our range as the greatest distance between a duct exit point and Palmer Station for which we can identify a whistler which would have had an equatorial field $\geq$6 pT. A conservative threshold for the weakest routinely detectable whistlers at Palmer Station might be 5 μV/m. Applying the method used earlier, we find that a whistler with an equatorial duct field of 6 pT would reach Palmer Station at this detection threshold if the duct exit point were 2500 km from Palmer Station. Palmer Station should thus be able to detect 95% of whistlers exiting ducts within 2500 km. This assumes that the downcoming whistlers illuminate the Earth-ionosphere waveguide equally in all directions, which may not be a good assumption; *Helliwell* [1965] showed that VLF waves would tend to propagate toward the geomagnetic pole when leaving a duct. On the other hand, since we are concerned with $2 < L < 3$, and since Palmer Station lies at $L = 2.4$, this effect would only lead to a conservative undercount of $2.4 < L < 3$ whistlers.

Assuming that a ducted whistler induces radiation belt losses only from within its duct, we will average precipitation flux from the area of a single duct (A_{duct}) over the area of the entire monitored region (A_{region}). Using our range estimate above, the region over which Palmer Station could detect precipitation-associated whistlers would be 5000 km wide between $L = 2$ and $L = 3$, or about 6,600,000 km^2 at 100 km altitude (Figure 22). Scaling *Angerami*'s [1970] estimate of the cross-sectional area of a duct to

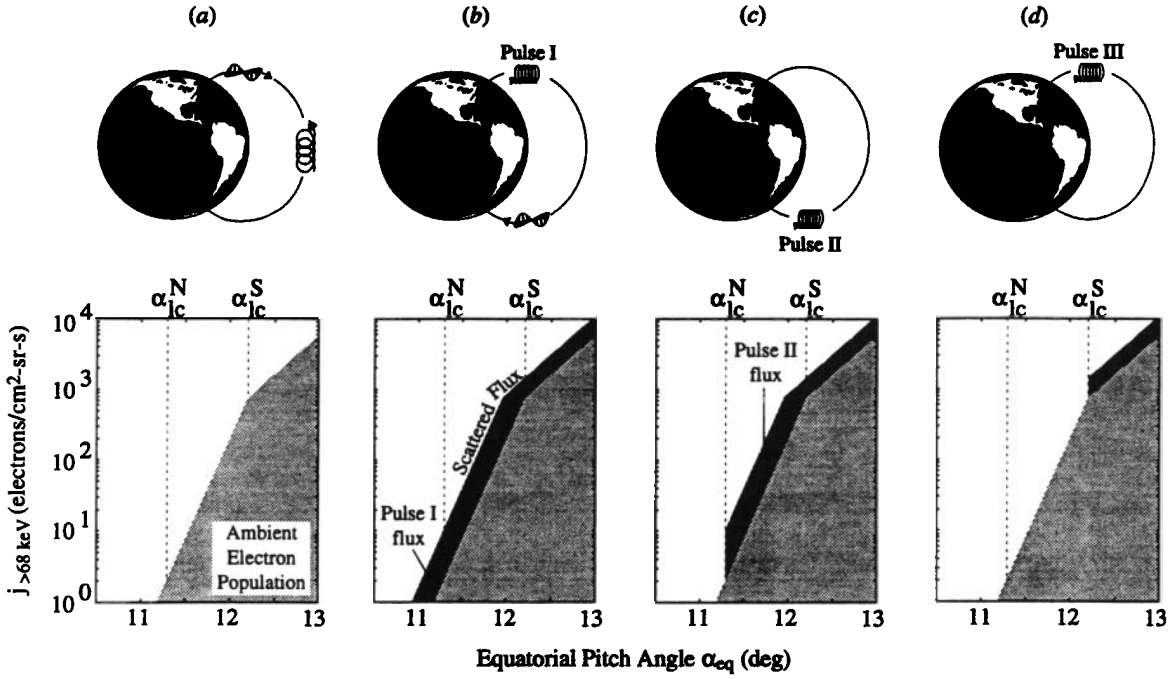

Fig. 20. The effect of the South Atlantic magnetic anomaly on electron precipitation from the radiation belts. (*a*) The anomaly results in two loss cones: electrons with equatorial pitch angles inside the northern loss cone ($\alpha_{eq} < \alpha_{lc}^N$) precipitate in the northern hemisphere, while those with pitch angles inside the southern loss cone ($\alpha_{eq} < \alpha_{lc}^S$) precipitate in the southern hemisphere. (*b*) When loss-cone electrons are pitch-angle scattered by a whistler, the total additional electron flux inside the northern loss cone is orders of magnitude less than that inside the southern loss cone, so that pulse I may be far smaller than (*c*) pulse II. (*d*) Pulses III and beyond would consist primarily of backscattered electrons. The ambient population profile is adapted from Figure 3 of *Inan et al.* [1988*c*].

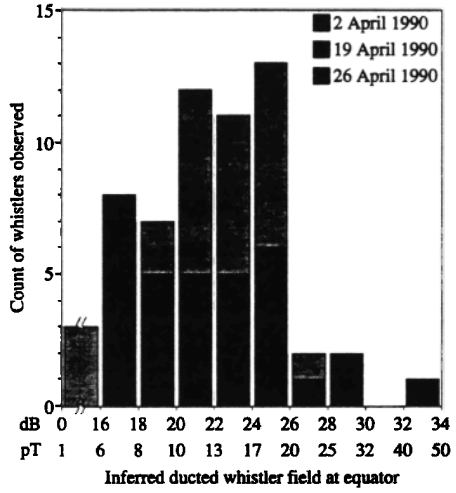

Fig. 21. Equatorial ducted whistler wave magnetic fields inferred from ground measurements of 59 whistlers on 3 different days. The average equatorial ducted field (B_{dw}) is 12 pT. A feature of the data from all 3 days is a noticeable drop in the number of whistlers observed over 20 pT, possibly indicating a threshold in the efficiency with which lightning generates radio atmospherics and/or ducted whistlers.

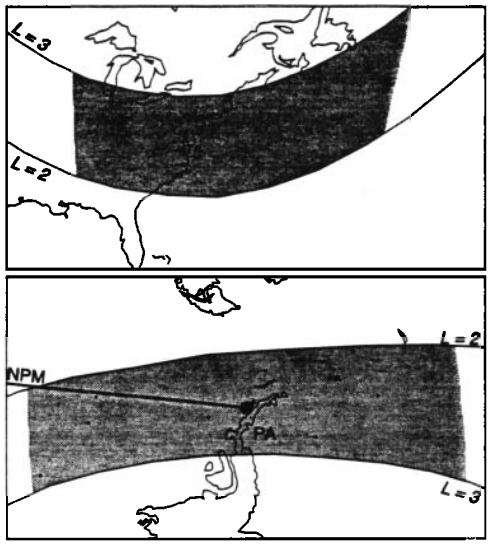

Fig. 22. The region monitored for whistler-induced precipitation by Palmer Station, Antarctica. The shaded region in the lower panel indicates the 5000-km-wide area between $L = 2$ and $L = 3$, discussed in the text, within which 95% of whistlers exiting ducts would be detected at Palmer Station. The geomagnetic conjugate of this area is shaded in the upper panel. For the purpose of illustration, the endpoints of ducts guiding a hypothetical 10-path whistler are shown as dots about 30 km in diameter scattered arbitrarily throughout the region. One duct endpoint is pictured close to the NPM–PA path, where precipitation spatially associated with that duct might cause a signal-perturbing ionospheric disturbance. The evidence in this paper suggests that every multipath whistler results in multiple small precipitation zones, located at the conjugate endpoints of excited ducts and spread over thousands of kilometers.

100 km altitude gives 370 km^2. Thus the fraction of the monitored area covered by a single duct is $A_{duct}/A_{region} \simeq 6 \times 10^{-5}$.

Belt Losses for a Representative Whistler Component

We now estimate the percentage of flux lost from a duct due to precipitation by an average whistler component, which we will write as Φ_{loss}/Φ_{duct}. The best starting point appears to be S81-1 satellite observations reported by *Voss et al.* [1984], who found

a precipitation loss of omnidirectional flux density of ~0.001% in association with a whistler measured at Palmer Station to be 15 μV/m at 1.5 kHz [*Inan et al.*, 1989]. The whistler and precipitation pulse were marked as event "D" by *Voss et al.* [1984]. We use this reported flux loss percentage with caution; it represents only a single case and is uncertain by a factor of ~2 because S81-1 was unable to directly observe southern loss-cone electrons mirroring above it and because much of the precipitating flux it did observe was at the edge of the detectors' field of view (M. Walt, private communication, 1992). Furthermore, to use this finding as a reference, we must assume that the satellite was measuring scattered electrons from within a duct and that the whistler observed at Palmer Station had propagated in that duct and caused that scattering. We consider the validity of these assumptions one at a time.

During the 40-s period discussed by *Voss et al.* [1984] the S81-1 satellite observed four precipitation bursts over a distance of ~290 km. *Angerami* [1970] estimated the horizontal extent of ducts to be 15–27 km at 300 km altitude, and at the 230 km altitude of the S81-1 satellite, such ducts would be only a couple of kilometers smaller. It is not unreasonable that four ducts of this size may have been coincidentally clustered in the region traversed by the satellite, especially when one considers that back-to-back examples of precipitation are rare in the S81-1 data (H. D. Voss, private communication, 1992). Such clustering of ducts appears to be possible: the April 19, 1990 data discussed in section 5 were consistent with multiple ducts in the vicinity of Huntsville (which, interestingly, is located only ~350 km from the ground trajectory of the S81-1 satellite during the *Voss et al.* [1984] measurements).

If the observed precipitation were indeed confined to ducts, however, those ducts may have been larger than suggested above. The 8 km/s speed of the S81-1 satellite would bring it from one edge of a 24-km duct to the other in 3 s, yet in the four events reported by *Voss et al.* [1984] the precipitation bursts were observed to last 3–5 s. We could infer somewhat larger ducts to account for the 5-s observations, say ~40 km, but even then it is unlikely that the satellite's time in a duct and the duration of precipitation would so closely coincide 4 times in a row. These considerations may indicate that *Angerami* [1970] underestimated the horizontal extent of ducts and that a closer estimate might be 60–70 km at 230-km altitude. If ducts and ionospheric disturbances are linked, as suggested in this paper, this estimate is consistent with the <100 km extent of whistler-associated disturbances reported by *Carpenter and LaBelle* [1982] and *Inan et al.* [1990]. Such duct sizes would increase the A_{duct}/A_{region} ratio nearly tenfold.

Even if we take the ducts for granted, it is not obvious that the whistler component whose intensity was recorded at Palmer Station was responsible for the precipitation in event D. If there were several ducts, the measured intensity might correspond to a whistler propagating in any one of them.

Laying this reservation aside for the moment, we can estimate the equatorial intensity of the ducted whistler using the method developed earlier. Given that the foot of the satellite's $L = 2.24$ field line (and therefore presumably the foot of the duct) was about 1800 km from Palmer Station, the equatorial duct field corresponding to 15 μV/m on the ground would have been about 34 pT. When compared with the other duct fields obtained earlier with the same method (Figure 21), 34 pT is almost 3 times the average field and is in the top 3% of observed field strengths. Since precipitation event D discussed by *Voss et al.* [1984] was also unusually strong, in the top 10%, compared with others observed on S81-1 (H. D. Voss, private communication, 1992), it is at least not inconsistent with the available data to associate the observed whistler intensity with event D.

With this reference associating a duct field (34 pT) with belt losses in the duct (0.001%) at $L = 2.24$, we can estimate losses associated with more typical whistlers. Because scattering is thought to be linearly related to wave field under these circumstances [*Inan et al.*, 1982; *Chang and Inan*, 1985], the "average" precipitation-inducing whistler, at 12 pT, might cause a loss of $\Phi_{loss}/\Phi_{duct} \simeq 0.0004\%$ in omnidirectional flux density in a duct at $L = 2.24$.

The absolute equatorial wave fields just discussed may not be accurate: in a case study of event D, *Inan et al.* [1989] found that the best agreement between scattering theory and the *Voss et al.* [1984] precipitation observations was obtained with equatorial fields of 200 pT. The order-of-magnitude discrepancy may reflect deficiencies in the scattering model or uncertainty in our assumptions concerning ionospheric and subionospheric wave propagation losses. Nevertheless, since both our reference (34 pT) and test (12 pT) equatorial fields were calculated in the same way, their relative strength should still be useful.

Whistler Occurrence Statistics

Table 3 lists average values for whistler rate (W) observed during a 5-year survey by *Laaspere et al.* [1963] at Port Lockroy, a site about 30 km from Palmer Station. Since the survey counted whistlers by ear, it seems certain that multipath whistlers were interpreted as single events; therefore, because each whistler component might cause precipitation, we must multiply the whistler counts by a representative value for ducted components per whistler (N_d). Familiarity with Palmer Station data leads us to suggest an average of $N_d = 10$ components per whistler,

TABLE 3. Whistler Rates and Inferred Electron Lifetimes

Local Conditions	Whistler Rate W, min^{-1}	Component Rate, min^{-1}	Electron τ, days[a]
Extreme day[b]	195	1560	2×10^3
Average winter night[c]	22	220[d]	1×10^4
Average winter day[c]	4	40[d]	7×10^4
Average summer night[c]	2.4	24[d]	1×10^5
Average summer day[c]	0.3	3[d]	1×10^6
Year-round average[e]	6	60[d]	5×10^4

[a] Calculated for $L = 2.24$.
[b] Palmer Station, Antarctica, April 2, 1990, about 2200 UT.
[c] Port Lockroy, Antarctica, from *Laaspere et al.* [1963].
[d] Assuming an average of $N_d = 10$ components per whistler.
[e] Port Lockroy, Antarctica, averaged from *Laaspere et al.* [1963].

leading to the corresponding whistler component rates which are also given in Table 3. If only a single loop antenna were used at Port Lockroy, weak whistlers arriving from unpropitious directions relative to the plane of the antenna may have been missed. Whistler rates presented in Table 3 may therefore underestimate the total occurring in the monitored region.

Electron Lifetime Estimates

We can now estimate a representative percentage of radiation belt flux lost per minute. In calculating this value, we assume that over the long term the N_d excited ducts are distributed uniformly with respect to L in the monitored region. This allows us to treat the quantity $N_d \times (A_{\text{duct}}/A_{\text{region}})$ as an effective "duct density" which is applicable for any chosen L and corresponding value of $\Phi_{\text{loss}}/\Phi_{\text{duct}}$. Choosing an annual average of six whistlers per minute for W from Table 3 and using $N_d = 10$, we have

$$\left(\frac{\Phi_{\text{loss}}}{\Phi_{\text{duct}}}\right)\left(\frac{A_{\text{duct}}}{A_{\text{region}}}\right)(W)(N_d) \simeq 1 \times 10^{-6} \text{ \% min}^{-1} \quad (1)$$

loss of omnidirectional flux density at $L = 2.24$, where

N_d number of components per whistler, that is, the number of excited ducts;
W whistler occurrence rate (per minute);
$\frac{A_{\text{duct}}}{A_{\text{region}}}$ fraction of the monitored area covered by a single duct; and
$\frac{\Phi_{\text{loss}}}{\Phi_{\text{duct}}}$ percent loss of omnidirectional flux density in a duct per whistler.

To compare this result with loss rates predicted for other radiation belt processes, we express it as an energetic electron lifetime τ. We define τ as the time in which the belt electron population at a given L in the monitored region would drop to $1/e$ of its original density, assuming that pitch angle diffusion near the loss cone is adequate to maintain the percentage loss of omnidirectional flux per minute, but ignoring other source or loss processes. On the basis of the flux loss percentage just estimated, we calculate the annual average electron lifetime τ to be $\sim 5 \times 10^4$ days, or about 140 years, at $L = 2.24$. Lifetimes for other whistler rates are given in Table 3. Note that if the horizontal extent of ducts is 3 times *Angerami*'s [1970] estimate, as discussed earlier, these lifetime estimates would drop almost an order of magnitude.

We can compare this result to a theoretical lifetime prediction based on a "coherent diffusion coefficient" $D^c_{\alpha\alpha}$ introduced by *Inan* [1987] to describe pitch angle diffusion of belt electrons as a result of interactions with ducted whistler mode signals. Accounting for the localized and episodic nature of scattering by ducted whistlers, the analysis gives $\tau \simeq 2.7 \times 10^4$ days at $L = 2.24$, encouragingly similar to the empirical result. The details of this analysis are given in the appendix. Note that both the empirical and theoretical lifetime inferences depend on $A_{\text{duct}}/A_{\text{region}}$, W, N_d, and the equatorial ducted whistler wave field B_{dw}.

The predicted electron lifetimes can also be compared with theoretical lifetime estimates based on scattering by nonducted plasmaspheric hiss, which were suggested by *Lyons and Thorne* [1973] to explain the equilibrium of the radiation belts. The τ for such losses at $L = 2.24$ presented by *Lyons and Thorne* [1973, Figure 1] ranges from $\sim 10^5$ days for 90-keV electrons to 10^3 days for 600-keV electrons. The resemblance between these lifetimes and those estimated for ducted whistler-induced losses indicates that, at $L = 2.24$, losses of ~70- to ~200-keV electrons induced by ducted whistlers and by plasmaspheric hiss may be similar. If the suggestion by *Lyons and Thorne* [1973] that plasmaspheric hiss controls radiation belt equilibrium in the plasmasphere is correct, this analysis would indicate that ducted whistlers may share significantly in that control.

The hiss-related lifetimes modeled by *Lyons and Thorne* [1973] decrease with increasing L. The model predicts, for example, that the lifetime of a 100-keV belt electron will drop roughly a thousandfold between $L = 2$ and $L = 3$. The increasing efficiency of wave-particle scattering which is responsible for this drop would similarly affect interactions involving ducted whistlers. In their model of precipitation by ducted whistlers, *Chang and Inan* [1985] predicted over an order of magnitude increase in the total energy deposition of precipitation bursts from $L = 2$ to $L = 3$, while at the same time whistler-resonant electron energies fall about an order of magnitude. Together these two effects mean a hundredfold increase in the density of precipitating burst electrons. Considering the order-of-magnitude drop in the belt population density of 120–240 keV electrons from $L = 2$ to $L = 3$ [*Lyons and Williams*, 1975*a*], the total effect is a thousandfold increase in the percentage belt loss induced by whistlers. This, in turn, means a thousandfold decrease in whistler-associated belt electron lifetimes, similar to that expected for hiss. Losses of ~70- to ~200-keV belt electrons inferred to be caused by ducted whistlers and by hiss would thus appear to be comparable across the entire $2 < L < 3$ range.

Discussion

Satellite studies of radiation belt recovery after geomagnetic storms and upper atmosphere nuclear weapons tests have yielded evidence of very short electron lifetimes. Following an intense storm in November 1968, for example, *West et al.* [1981] reported Ogo 5 satellite observations of $\tau = 49$ days for 158-keV electrons at $L = 2.4$. Although *West et al.* [1981] pointed out the consistency of their experimental results with theoretical hiss-related lifetimes presented in Figure 7 of *Lyons et al.* [1972], such short lifetimes do not agree with the quiet time hiss-induced losses suggested by *Lyons and Thorne* [1973] nor with the ducted whistler-induced losses estimated in this paper.

The wide range of predicted values for hiss-related lifetimes results primarily from differences in total wave intensity (B_w) used in the hiss-induced loss model. While *Lyons and Thorne* [1973] found that $B_w = 10$ pT led to an accurate prediction of quiet time radiation belt populations inside the plasmasphere, *Lyons et al.* [1972] used $B_w = 35$ pT to predict the short lifetimes later corroborated by *West et al.* [1981]. In the context of the model offered by *Lyons and Thorne* [1973], however, $B_w = 35$ pT is inconsistent with the quiet time structure of the radiation belts. For example, if $B_w = 35$ pT had been used instead of $B_w = 10$ pT to model the ambient quiet-time population for 500-keV electrons at $L = 2$, the resulting population prediction would have been over 5 orders of magnitude less [*Lyons and Thorne*, 1973].

Therefore, if hiss- and whistler-induced losses are responsible for the short electron lifetimes observed following injection events, the equilibrium loss rates just discussed would have to rise during injection recovery. *Smith et al.* [1974] have documented elevated poststorm values of B_w, suggestive of such an increase in hiss-induced losses, and poststorm increases in ducted whistler rates have also been observed [*Andrews*, 1975]. The tandem intensification of hiss-induced and whistler-induced losses after storms would be consistent with the suggestion by *Lyons and Williams* [1975*b*] that the relative strengths of source and loss processes remain the same before and after injection events. On the

other hand, it is possible that neither hiss- nor whistler-induced losses dominate the radiation belts because an interdependence between loss rates and belt population would be inconsistent with the observed exponential character of poststorm belt recoveries [*West et al.*, 1981].

We emphasize that these preliminary results apply only to the region monitored by Palmer Station (Figure 22), an area which is not typical of other longitudes. The region is conjugate to frequent thunderstorm activity in the eastern United States, which may partly explain the observation near Palmer Station of what are possibly the world's highest whistler rates [*Laaspere et al.*, 1963]. The presence of the South Atlantic magnetic anomaly in the same area means that our loss rate estimates may have been augmented by drift losses at these particular longitudes. Nevertheless, the shaded regions in Figure 22 account for over one fifth of the Earth's surface between $L = 2$ and $L = 3$. Even if whistler-induced precipitation were completely absent elsewhere, a factor of 5 in the lifetimes listed in Table 3 would not affect the first-order conclusions offered herein.

Though we do not consider regions below $L = 2$, above $L = 3$, or outside the plasmapause in our lifetime estimates, whistler-associated precipitation of >50-keV electrons does appear to occur in these regions [*Carpenter and Inan*, 1987]; in general, however, such precipitation is more difficult to detect with our ground-based approach. Below $L = 2$, whistler-resonant electron energies reach into a few MeV, but the relatively small belt population of such high-energy electrons, several orders of magnitude less than that for electrons of a few hundred keV [*West et al.*, 1981], substantially reduces the total energy of whistler-induced precipitation bursts [*Chang and Inan*, 1985]. Between $L = 3$ and the plasmapause, declining whistler-resonant energies and belt populations reduce the precipitation flux of >50-keV electrons, although the precipitation flux of lower-energy electrons increases [*Chang and Inan*, 1985]. Whistler-resonant energies in the diminished cold plasma densities beyond the plasmapause are >50 keV, and burst precipitation of such electrons in association with whistler-triggered emissions has been reported [*Rosenberg et al.*, 1971; *Dingle and Carpenter*, 1981; *Carpenter et al.*, 1985]; however, the relative significance of ducted whistlers, whistler-triggered emissions, and spontaneous emissions such as chorus [*Burtis and Helliwell*, 1976] as belt loss processes in these regions is not known.

The evidence of a strong link between precipitation and whistler ducts supports the suggestion by *Bernhardt and Park* [1977] that ducts, once formed, may be self-reinforcing. The confinement of ionizing precipitation bursts to a small ionospheric region at the foot of the duct may increase the local ionospheric pressure above the nighttime ambient and thus help maintain the duct enhancement. The process by which ducts are initially formed is still unclear, although thunderstorms may be involved. The precipitation of 10-eV to 40-keV electrons induced by nonducted whistlers above a thunderstorm [*Inan and Bell*, 1991] and electric fields from the cloud charging which precedes lightning [*Park and Helliwell*, 1971] have both been suggested to cause localized ionization adequate to form duct enhancements.

Indeed, lightning may contribute to all of the magnetospheric processes discussed in this paper. In addition to its possible role in the formation of ducts and its triggering of belt losses via ducted whistlers, lightning may also induce losses of lower-energy electrons via nonducted whistlers [*Jasna et al.*, 1992] and has been suggested as a source of plasmaspheric hiss [*Draganov et al.*, 1992].

8. SUMMARY

We have presented detailed evidence of a close association between individual whistler ducts and conjugate ionospheric disturbances sensed by the perturbation of subionospheric VLF, LF, and MF signals. We summarize this evidence as follows:

1. Even barely detectable whistlers (~2 μV/m) can be associated with ionospheric disturbances in both hemispheres.

2. A case study showed slow-onset and "overshoot" perturbation signatures to be consistent with multiple ionospheric disturbances associated one-to-one with individual components of multipath ducted whistlers.

3. Two case studies of whistler component arrival azimuths demonstrated a correspondence between duct exit locations and the locations of ionospheric disturbances inferred from configurations of perturbed subionospheric signal paths.

4. The behavior of signal perturbation onsets as a function of time compared well with predictions for conjugate precipitation pulses induced by ducted whistler scattering of radiation belt electrons.

This evidence casts lightning in the role of trigger for a magnetospheric "shotgun": for each of the multiple ducts excited simultaneously by a typical multipath whistler, there may be a series of precipitation bursts which strike the ionosphere in geomagnetically conjugate regions. Since sferics can couple into ducts over 2500 km from the source discharge [*Carpenter and Orville*, 1989], a lightning flash over Huntsville, for example, has the potential to cause localized precipitation bursts and ionospheric disturbances over the entire contiguous United States as well as over the conjugate region in the southern hemisphere. The occurrence of such simultaneous precipitation bursts distributed over a wide area is consistent with the satellite observation by *Voss et al.* [1984] of precipitation 2000 km west of Palmer Station when whistler-associated perturbations of NAA–PA suggested precipitation to the north of Palmer Station.

Belt losses caused by ducted whistlers can be estimated to first order, based on the hypothesis that every ducted whistler component scatters and precipitates radiation belt electrons. The lifetimes of ~70- to ~200-keV electrons caused by this process are similar to those estimated by *Lyons and Thorne* [1973] due to precipitation by nonducted ELF/VLF hiss, which those authors suggested was sufficient to explain radiation belt structure. Ducted whistlers may therefore play a significant role in maintaining the equilibrium of energetic radiation belt electron populations.

APPENDIX: ELECTRON LIFETIME AT $L = 2.24$ DETERMINED FROM A COHERENT DIFFUSION COEFFICIENT

Inan [1987] introduced a "coherent diffusion coefficient" $D^c_{\alpha\alpha}$ to represent the electron pitch angle scattering efficiency of ducted whistler mode waves, which he defined in his equation (16) as

$$D^c_{\alpha\alpha} \equiv \frac{\langle(\Delta\alpha)^2\rangle}{T_r} \tag{2}$$

where $\Delta\alpha$ is the net total pitch angle change for each electron, the angular brackets denoting an average over the initial electron Larmor phase, and T_r is the "resonance time," the period over which most pitch angle scattering takes place during an electron's interaction with a wave.

For scattering induced by ducted whistlers, however, pitch angle diffusion is neither continuous nor uniformly distributed in space. We therefore introduce a temporal efficiency coefficient η_t which

represents the whistler-electron interaction time occurring per unit real time:

$$\eta_t \equiv \frac{T_r}{t} \tag{3}$$

and a spatial efficiency coefficient η_s which represents the fraction of space occupied by a single whistler duct, defined in terms of the estimated duct area and the area of the region monitored for ducts at 100 km altitude:

$$\eta_s \equiv \frac{A_{\text{duct}}}{A_{\text{region}}}. \tag{4}$$

Since the lifetime τ of belt electrons diffusing in pitch angle can be approximated as $\tau \simeq 1/D_{\alpha\alpha}$ [*Schulz and Lanzerotti*, 1974], we can estimate that for whistler-induced diffusion

$$\tau \simeq \frac{1}{D^c_{\alpha\alpha}\eta_t\eta_s}. \tag{5}$$

To find $D^c_{\alpha\alpha}$ and η_t at $L = 2.24$, we must first estimate T_r. Using a parallel resonance electron velocity $v_R = 1.8 \times 10^8$ m/s for a 136-keV whistler-resonant loss-cone electron at $L = 2.24$ [*Inan et al.*, 1989] in equation (15) of *Inan* [1987], we find the length of the interaction zone as 748 km. Dividing this distance by v_R gives $T_r \simeq 4.2$ ms.

Since $D^c_{\alpha\alpha}$ as described by equation (18) of *Inan* [1987] varies directly as T_r and as the square of equatorial ducted wave field B_{dw} and depends only weakly on other quantities such as L, we can scale the $L = 4$ $D^c_{\alpha\alpha}$ estimate from that paper. For $B_{dw} = 1$ pT and $T_r \simeq 52$ ms, *Inan* [1987] found $D^c_{\alpha\alpha} \simeq 1.46 \times 10^{-4}$ s^{-1}. Multiplying by the square of 12 pT (the average whistler B_{dw} estimated from Figure 21) and by 4.2 ms/52 ms, we obtain $D^c_{\alpha\alpha} \simeq 1.70 \times 10^{-3}$ s^{-1}.

To find η_t, we multiply 4.2 ms by an annual average of 60 whistler components per minute (Table 3) giving $\eta_t \simeq 0.0042$. We use the value for $\eta_s \simeq 6 \times 10^{-5}$ determined earlier in this paper. Solving equation (5) gives $\tau \simeq 2.3 \times 10^9$ s or 2.7×10^4 days.

The first-order similarity between this result and the values listed in Table 3 is encouraging; however, it must be interpreted cautiously. *Inan* [1987] used $D^c_{\alpha\alpha}$ to represent the scattering of equatorially resonant electrons, while more comprehensive estimates of precipitated flux account for electrons that interact with the wave elsewhere along the field line. In particular, although $D^c_{\alpha\alpha}$ depends on $(B_{dw})^2$, *Inan et al.* [1982] predicted that total precipitation flux would vary linearly with B_{dw} when particle trapping is neglected (which they estimated to be a good assumption for $B_{dw} \lesssim 30$ pT at $L \simeq 2.25$).

Acknowledgments. The authors gratefully acknowledge the support of our experiments by Gerald Fishman at Marshall Space Flight Center and by Colin Hines at the Arecibo Observatory. We would also like to thank A. J. Smith of the British Antarctic Survey, who furnished us with information on the VLF equipment used at Port Lockroy. We are deeply indebted to Martin Walt of Lockheed for his extensive and experienced counsel, and to Tim Bell, Don Carpenter, Sasha Draganov, Robert Helliwell and our other colleagues in the STAR Laboratory for many helpful comments and conversations. Bill Trabucco, Dave Shafer, and Jerry Yarbrough rendered critical and much appreciated assistance with field operations and data analysis. This research was sponsored by the Polar Programs Division of the National Science Foundation under grant DPP-9020687. Data acquisition was supported at Huntsville and at Lake Mistissini by the Atmospheric Sciences Division of the National Science Foundation under grant ATM-9113012, and at Arecibo by the Office of Naval Research under grant N00014-82-K-0489. Construction and installation of the Huntsville observatory were accomplished with the support of the National Aeronautics and Space Administration under grant NAG8-778.

The Editor thanks R. L. Dowden and another referee for their assistance in evaluating this paper.

REFERENCES

Andrews, M. K., Delayed storm-time increases in the whistler rate at mid-latitudes, *J. Atmos. Terr. Phys.*, *37*, 1423, 1975.

Angerami, J. J., Whistler duct properties deduced from VLF observations made with the Ogo 3 satellite near the magnetic equator, *J. Geophys. Res.*, *75*, 6115, 1970.

Berger, M. J., S. M. Seltzer, and K. Maeda, Some new results on electron transport in the atmosphere, *J. Atmos. Terr. Phys.*, *36*, 591, 1974.

Bernard, L. C., A new nose extension method for whistlers, *J. Atmos. Terr. Phys.*, *35*, 871, 1973.

Bernhardt, P. A., and C. G. Park, Protonospheric-ionospheric modeling of VLF ducts, *J. Geophys. Res.*, *82*, 5222, 1977.

Burgess, W. C., and U. S. Inan, Simultaneous disturbance of conjugate ionospheric regions in association with individual lightning flashes, *Geophys. Res. Lett.*, *17*, 259, 1990.

Burtis, W. J., and R. A. Helliwell, Magnetospheric chorus: occurrence patterns and normalized frequency, *Planet. Space Sci.*, *24*, 1007, 1976.

Carpenter, D. L., and U. S. Inan, Seasonal, latitudinal and diurnal distributions of whistler-induced particle precipitation events, *J. Geophys. Res.*, *92*, 3429, 1987.

Carpenter, D. L., and J. W. LaBelle, A study of whistlers correlated with bursts of electron precipitation near $L = 2$, *J. Geophys. Res.*, *87*, 4427, 1982.

Carpenter, D. L., and R. E. Orville, The excitation of active whistler mode signal paths in the magnetosphere by lightning: Two case studies, *J. Geophys. Res.*, *94*, 8886, 1989.

Carpenter, D. L., and R. L. Smith, Whistler measurements of electron density in the magnetosphere, *Rev. Geophys.*, *2*, 415, 1964.

Carpenter, D. L., U. S. Inan, M. L. Trimpi, R. A. Helliwell, and J. P. Katsufrakis, Perturbations of subionospheric LF and MF signals due to whistler-induced electron precipitation bursts, *J. Geophys. Res.*, *89*, 9857, 1984.

Carpenter, D. L., U. S. Inan, E. W. Paschal, and A. J. Smith, A new VLF method for studying burst precipitation near the plasmapause, *J. Geophys. Res.*, *90*, 4383, 1985.

Chang, H. C., and U. S. Inan, Lightning-induced electron precipitation from the magnetosphere, *J. Geophys. Res.*, *90*, 1531, 1985.

Cornwall, J. M., Scattering of energetic trapped electrons by very-low-frequency waves, *J. Geophys. Res.*, *69*, 1251, 1964.

Cousins, M. D., Direction finding on whistlers and related VLF signals, *Tech. Rep. 3432-2*, Stanford Electron. Labs., Stanford, Calif., 1972.

Crary, J. H., The effect of the Earth-ionosphere waveguide on whistlers, *Tech. Rep. 9*, p. 48, Stanford Electron. Labs., Stanford, Calif., 1961.

Daniell, G. J., Approximate dispersion formulæ for whistlers, *J. Atmos. Terr. Phys.*, *48*, 267, 1986*a*.

Daniell, G. J., Analytic properties of the whistler dispersion function, *J. Atmos. Terr. Phys.*, *48*, 271, 1986*b*.

Dingle, B., and D. L. Carpenter, Electron precipitation induced by VLF noise bursts at the plasmapause and detected at conjugate ground stations, *J. Geophys. Res.*, *86*, 4597, 1981.

Dowden, R. L., and C. D. D. Adams, Location of lightning-induced electron precipitation from measurement of VLF phase and amplitude perturbations on spaced antennas and on two frequencies, *J. Geophys. Res.*, *95*, 4135, 1990.

Draganov, A. B., U. S. Inan, V. S. Sonwalkar, and T. F. Bell, Magnetospherically reflected whistlers as a source of plasmaspheric hiss, *Geophys. Res. Lett.*, *19*, 233, 1992.

Dungey, J. W., Loss of Van Allen electrons due to whistlers, *Planet. Space Sci.*, *11*, 591, 1963.

Goldberg, R. A., S. A. Curtis, and J. R. Barcus, Detailed spectral structure of magnetospheric electron bursts precipitated by lightning, *J. Geophys. Res.*, *92*, 2505, 1987.

Helliwell, R. A., *Whistlers and Related Ionospheric Phenomena*, pp. 43, 56–58 and 71, Stanford University Press, Stanford, Calif., 1965.

Helliwell, R. A., J. P. Katsufrakis, and M. L. Trimpi, Whistler-induced amplitude perturbation in VLF propagation, *J. Geophys. Res.*, *78*, 4679, 1973.

Inan, U. S., Gyroresonant pitch angle scattering by coherent and incoherent whistler mode waves in the magnetosphere, *J. Geophys. Res.*, *92*, 127, 1987.

Inan, U. S., and T. F. Bell, Pitch angle scattering of energetic particles by oblique whistler waves, *Geophys. Res. Lett.*, *18*, 49, 1991.

Inan, U. S., and D. L. Carpenter, On the correlation of whistlers and associated subionospheric VLF/LF perturbations, *J. Geophys. Res.*, *91*, 3106, 1986.

Inan, U. S., and D. L. Carpenter, Lightning-induced electron precipitation

events observed at $L \sim 2.4$ as phase and amplitude perturbations on subionospheric VLF signals, *J. Geophys. Res., 92*, 3293, 1987.

Inan, U. S., T. F. Bell, and H. C. Chang, Particle precipitation induced by short-duration VLF waves in the magnetosphere, *J. Geophys. Res., 87*, 6243, 1982.

Inan, U. S., H. C. Chang, and R. A. Helliwell, Electron precipitation zones around major ground-based VLF signal sources, *J. Geophys. Res., 89*, 2891, 1984.

Inan, U. S., D. L. Carpenter, R. A. Helliwell, and J. P. Katsufrakis, Subionospheric VLF/LF phase perturbations produced by lightning-whistler induced particle precipitation, *J. Geophys. Res., 90*, 7457, 1985*a*.

Inan, U. S., H. C. Chang, R. A. Helliwell, W. L. Imhof, J. B. Reagan, and M. Walt, Precipitation of radiation belt electrons by man-made waves: a comparison between theory and measurement, *J. Geophys. Res., 90*, 359, 1985*b*.

Inan, U. S., W. C. Burgess, T. G. Wolf, and D. C. Shafer, Lightning-associated precipitation of MeV electrons from the inner radiation belt, *Geophys. Res. Lett., 15*, 172, 1988*a*.

Inan, U. S., D. C. Shafer, and W. Y. Yip, Subionospheric VLF signatures of nighttime D region perturbations in the vicinity of lightning discharges, *J. Geophys. Res., 93*, 11,455, 1988*b*.

Inan, U. S., T. G. Wolf, and D. L. Carpenter, Geographic distribution of lightning-induced electron precipitation observed as VLF/LF perturbation events, *J. Geophys. Res., 93*, 9841, 1988*c*.

Inan, U. S., M. Walt, H. D. Voss, and W. L. Imhof, Energy spectra and pitch angle distributions of lightning-induced electron precipitation: Analysis of an event observed on the S81-1 (SEEP) satellite, *J. Geophys. Res., 94*, 1379, 1989.

Inan, U. S., F. A. Knifsend, and J. Oh, Subionospheric VLF "imaging" of lightning-induced electron precipitation from the magnetosphere, *J. Geophys. Res., 95*, 17,217, 1990.

Jasna, D., U. S. Inan, and T. F. Bell, Precipitation of suprathermal (100 eV) electrons by oblique whistler waves, *Geophys. Res. Lett., 19*, 1639, 1992.

Laaspere, T., M. G. Morgan, and W. C. Johnson, Some results of five years of whistler observations from Labrador to Antarctica, *Proc. IEEE, 51*, 554, 1963.

Lohrey, B., and A. B. Kaiser, Whistler-induced anomalies in VLF propagation, *J. Geophys. Res., 84*, 5122, 1979.

Lyons, L. R., and R. M. Thorne, Equilibrium structure of radiation belt electrons, *J. Geophys. Res., 78*, 2142, 1973.

Lyons, L. R., and D. J. Williams, The quiet time structure of energetic (35–560 keV) radiation belt electrons, *J. Geophys. Res., 80*, 943, 1975*a*.

Lyons, L. R., and D. J. Williams, The storm and poststorm evolution of energetic (35–560 keV) radiation belt electron distributions, *J. Geophys. Res., 80*, 3985, 1975*b*.

Lyons, L. R., R. M. Thorne, and C. F. Kennel, Pitch-angle diffusion of radiation belt electrons within the plasmasphere, *J. Geophys. Res., 77*, 3455, 1972.

Park, C. G., and R. A. Helliwell, The formation by electric fields of field-aligned irregularities in the magnetosphere, *Radio Sci., 6*, 299, 1971.

Poulsen, W. L., T. F. Bell, and U. S. Inan, Three-dimensional modeling of subionospheric VLF propagation in the presence of localized *D* region perturbations associated with lightning, *J. Geophys. Res., 95*, 2355, 1990.

Poulsen, W. L., U. S. Inan, and T. F. Bell, A multiple-mode three-dimensional model of VLF propagation in the Earth-ionosphere waveguide in the presence of localized D Region disturbances, *J. Geophys. Res., 98*, 1705, 1993.

Press, W. H., B. P. Flannery, S. A. Teukolsky, and W. T. Vetterling, *Numerical Recipes in C: The Art of Scientific Computing*, pp. 542–547, Cambridge University Press, Cambridge, 1988.

Rees, M. H., Auroral ionization and excitation by incident energetic electrons, *Planet. Space Sci., 11*, 1209, 1963.

Rosenberg, T. J., R. A. Helliwell, and J. P. Katsufrakis, Electron precipitation associated with discrete very low frequency emissions, *J. Geophys. Res., 76*, 8445, 1971.

Rycroft, M. J., Enhanced energetic electron intensities at 100 km altitude and a whistler propagating through the plasmasphere, *Planet. Space Sci., 21*, 239, 1973.

Schulz, M., and L. J. Lanzerotti, *Particle Diffusion in the Radiation Belts*, p. 78, Springer-Verlag, New York, 1974.

Smith, E. J., A. M. A. Frandsen, B. T. Tsurutani, R. M. Thorne, and K. W. Chan, Plasmaspheric hiss intensity variations during magnetic storms, *J. Geophys. Res., 79*, 2507, 1974.

Strangeways, H. J., Systematic errors in VLF direction-finding of whistler ducts, I, *J. Atmos. Terr. Phys., 42*, 995, 1980.

Strangeways, H. J., The upper cut-off frequency of nose whistlers and implications for duct structure, *J. Atmos. Terr. Phys., 53*, 151, 1991.

Strangeways, H. J., and M. J. Rycroft, Systematic errors in VLF direction-finding of whistler ducts, II, *J. Atmos. Terr. Phys., 42*, 1009, 1980.

Strangeways, H. J., M. J. Rycroft, and M. J. Jarvis, Multi-station VLF direction-finding measurements in eastern Canada, *J. Atmos. Terr. Phys., 44*, 509, 1982.

Tarcsai, Gy., H. J. Strangeways, and M. J. Rycroft, Error sources and travel time residuals in plasmaspheric whistler interpretation, *J. Atmos. Terr. Phys., 51*, 249, 1989.

Tsuruda, K., S. Machida, T. Terasawa, A. Nishida, and K. Maezawa, High spatial attenuation of the Siple transmitter signal and natural VLF chorus observed at ground-based chain stations near Roberval, Quebec, *J. Geophys. Res., 87*, 742, 1982.

Tsyganenko, N. A., A magnetospheric magnetic field model with a wrapped tail current sheet, *Planet. Space Sci., 37*, 5, 1989.

Vampola, A. L., Electron precipitation in the vicinity of a VLF transmitter, *J. Geophys. Res., 92*, 4525, 1987.

Voss, H. D., W. L. Imhof, M. Walt, J. Mobilia, E. E. Gaines, J. B. Reagan, U. S. Inan, R. A. Helliwell, D. L. Carpenter, J. P. Katsufrakis, and H. C. Chang, Lightning-induced electron precipitation, *Nature, 312*, 740, 1984.

West, H. I., Jr., R. M. Buck, and G. T. Davidson, The dynamics of energetic electrons in the Earth's outer radiation belt during 1968 as observed by the Lawrence Livermore National Laboratory's spectrometer on Ogo 5, *J. Geophys. Res., 86*, 2111, 1981.

Wolf, T. G., Remote sensing of ionospheric effects associated with lightning using very low frequency radio signals, Ph.D. thesis, Stanford University, Stanford, Calif., 1990.

Wolf, T. G., and U. S. Inan, Path-dependent properties of subionospheric VLF amplitude and phase perturbations associated with lightning, *J. Geophys. Res., 95*, 20,997, 1990.

Yip, W.-Y., U. S. Inan, and R. E. Orville, On the spatial relationship between lightning discharges and propagation paths of perturbed subionospheric VLF/LF signals, *J. Geophys. Res., 96*, 249, 1991.

W. C. Burgess, Department of Applied Ocean Physics and Engineering, Woods Hole Oceanographic Institution, Woods Hole, MA 02543.

U. S. Inan, STAR Laboratory, Department of Electrical Engineering, Stanford University, Stanford, CA 94305.

(Received December 1, 1992;
revised March 31, 1993;
accepted April 28, 1993.)